JUNE 2013

SAN FRANCISCO ESTUARY & WATERSHED SCIENCE
Sponsored by the Delta Science Program and the UC Davis John Muir Institute of the Environment

Hydrodynamic Simulation of Circulation and Residence Time in Clifton Court Forebay

Michael L. MacWilliams[1] and Edward S. Gross[2]

ABSTRACT

Circulation in Clifton Court Forebay (CCF) was simulated using the three-dimensional (3–D) hydrodynamic model UnTRIM. These numerical simulations were performed to provide a better understanding of circulation patterns, flow pathways, and residence time in Clifton Court Forebay in support of ongoing studies of pre-screen loss and fish facility efficiency for delta smelt (*Hypomesus transpacificus*) at the California State Water Project (SWP) export facilities. The 3–D hydrodynamic model of CCF was validated through comparisons to observed water surface elevations inside CCF, and comparisons to observed drifter paths and velocity measurements collected by the U.S. Geological Survey as part of this study. Flow measurements collected near the radial gates for 2 days during relatively low inflows suggest that the Hills (1988) gate equations may over-estimate inflow by as much as 39% when the CCF radial gates are only partially opened. Several alternative approaches to improve the implementation of the radial gate flows in the UnTRIM model were evaluated. The resulting model accurately predicts water surface elevations and currents inside CCF over a range of wind and operating conditions. The validated model was used to predict residence time and other transport time scales for two 21-day simulation periods, one of very low daily SWP export pumping averaging 19.3 m^3 s^{-1} and one for moderate daily SWP export pumping averaging 66.6 m^3 s^{-1}. The average transit time, indicating the time from entering CCF to reaching the fish facility, was estimated as 9.1 days for low export conditions and 4.3 days for moderate export conditions. These transport time scale estimates may be used to inform estimates of pre-screen losses inside CCF due to predation or other causes.

KEY WORDS

Sacramento–San Joaquin Delta, hydrodynamics, three-dimensional modeling, residence time, delta smelt, entrainment, particle tracking, State Water Project.

INTRODUCTION

Clifton Court Forebay (CCF) is a regulating reservoir in the southern Sacramento–San Joaquin Delta (south Delta) which is used to improve operations of the California State Water Project (SWP) Harvey O. Banks Pumping Plant (Banks Pumping Plant) and water diversions to the California Aqueduct (Clark et al. 2009). CCF has an area of approximately 900 ha. CCF storage ranges between 18.5 and 29.6 million m^3 (15,000 and 24,000 ac-ft), depending on water level within CCF (Kano 1990). Inflows to CCF are controlled by five radial gates; each gate is 6-m wide and 6-m tall. The maximum allowable flow through

1 Corresponding author: Delta Modeling Associates, Inc., P.O. Box 225174, San Francisco, CA 94122-5174; *michael@deltamodeling.com*
2 Resource Management Associates, Inc., 2039 Shattuck Avenue, #300, Berkeley, CA 94704

the gates is 340 $m^3 s^{-1}$ (12,000 cfs) to prevent scour in the Delta channels leading to CCF (Hills 1988). The radial gates are generally operated to allow inflows into CCF during high water and to minimize effects on south Delta water levels during low tides. Outflows from CCF include water exports from the Banks Pumping Plant to the SWP and from CCF to the Byron Bethany Irrigation District (BBID). The Banks Pumping Plant has a daily export capacity of about 15.7 million m^3 (12,700 ac-ft), however continuous operation is limited by the water level in CCF, and the highest pumping rates typically occur during periods of off-peak power demand (Kano 1990). Figure 1 is a map of the southern Sacramento–San Joaquin Delta, showing the locations of the CCF, the radial gates, the John E. Skinner Delta Fish Protective Facility (SFPF), and the Banks Pumping Plant.

The SFPF was designed to protect fish from entrainment into the California Aqueduct, and to safely return salvaged fish to the Delta (Clark et al. 2009). However, fish that enter CCF through the radial gates must travel a minimum of 4.0 km across CCF before reaching the SFPF. Fish species of the highest concern at this writing are listed through the Endangered Species Act as endangered or threatened species, and include delta smelt, longfin smelt, and Chinook salmon. Losses of fish during movement from the radial gates to the SFPF, termed pre-screen loss, include predation by fish and birds (Clark et al. 2009) and mortality due to temperature (Bennett 2005). One of the objectives of this study is to better understand the residence time of the fish inside CCF and the typical distance that they travel between the radial gates and the SFPF. Ultimately, the findings from this study should help in managing pre-screen losses of species of concern.

Estimates of the proportion of the larval and juvenile delta smelt population lost to water export in the Sacramento–San Joaquin Delta during the years 2001 to 2003 were as high as 25%, and contained large uncertainty (Kimmerer 2008). Perhaps the largest source of uncertainty in the Kimmerer (2008) estimates of delta smelt population losses is the uncertainty in pre-screen losses. The U.S. Fish and Wildlife Service (USFWS) has initiated several mark–recapture studies inside CCF to evaluate entrainment losses of juvenile and adult delta smelt at the SWP from exports in the south Delta (CALFED 2009). Mass mark–recapture studies of adult delta smelt were conducted in February and March 2009, and mark–recapture studies of juvenile delta smelt were conducted in June 2008 and June 2009 (Castillo et al. 2012). This study reported fish facility efficiency defined as the percent of the fish released at the entrance to the SFPF that were recaptured at the SFPF for each delta smelt release. The pre-screen losses, defined as fish losses in CCF before the SFPF entrance, were reported for each delta smelt release. During the February mark–recapture study, the estimated pre-screen losses were 94.3% and the estimated fish facility efficiency was 53.2%. During the March mark–recapture study, the estimated pre-screen losses were 99.1% and the estimated fish facility efficiency was 44.0%. During the June mark–recapture study, 99.9% pre-screen losses and 24.0% fish facility efficiency were estimated. Therefore, observed pre-screen losses were both large and highly variable.

Flows and transport processes in the Delta have been studied in several field studies (e.g., Smith et al. 1995; Oltmann and Simpson 1997) and hydrodynamic modeling efforts (e.g., CDWR 2005; Flow Science Inc. 2005; Smith et al. 2005; RMA 2005; USBR 2008; MacWilliams et al. 2009). Furthermore, studies of delta smelt entrainment losses suggest that hydrodynamics in the Delta substantially affects estimated entrainment (Grimaldo et al. 2009). In contrast, relatively little is known about hydrodynamics and transport inside CCF. The estimates of flow pathways and residence time inside CCF from detailed hydrodynamic modeling conducted as part of this study provide insight into the amount of time fish, such as delta smelt, may remain in CCF before they reach the fish facility. Residence time can be used to estimate the variability of pre-screen losses inside CCF with export flow and may help explain some of the observed variability in pre-screen losses. In addition, accurate simulation of hydrodynamics and water levels inside CCF validates that the CCF implementation used in the larger UnTRIM (Unstructured nonlinear

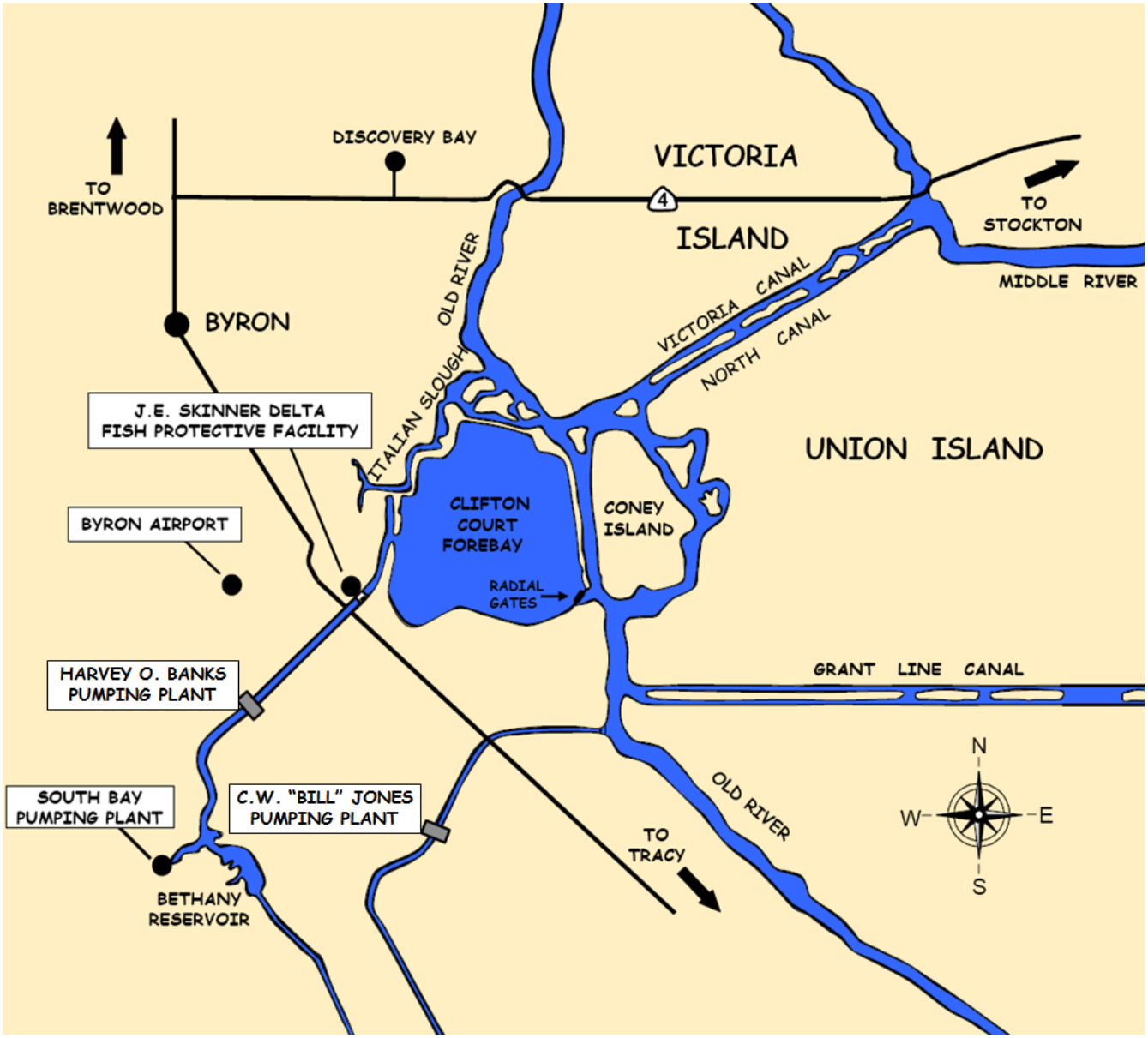

Figure 1 Map of the southern Sacramento–San Joaquin Delta, showing Clifton Court Forebay, the radial gates, the J. E. Skinner Delta Fish Protective Facility, and the Harvey O. Banks Pumping Plant. Source: J. Morinaka, California Department of Fish and Wildlife.

Tidal Residual Inter-tidal Mudflat) Bay–Delta Model (MacWilliams et al. 2008, 2009) accurately represents the effects of CCF inflows on flow and water levels in the south Delta.

METHODS

A high-resolution model of CCF was developed using the UnTRIM hydrodynamic model (Casulli and Zanolli 2002, 2005; Casulli 2009). The model was validated using field observations of water level and velocity, and through comparison to drifter data during two simulation periods in 2008 and 2009. The model was then used to develop a conceptual model for circulation within CCF for a range of flow and wind conditions, and to provide estimates of residence time inside CCF.

The first simulation period spans from June 1 through July 12, 2008, and was selected to coincide with a period of extensive data collection in CCF by the U.S. Geological Survey (USGS). The second simulation period spans from September 1, 2008 through April 30, 2009, and corresponds to two consecutive Acoustic Doppler Current Profiler (ADCP) deployments in CCF by the USGS. Total daily water exports during water years 2008 and 2009 were generally lower than the historical mean (Rossiter 2010). Le (2008) reports that water exports at the SWP and CVP were typical during April through June 2008 to meet water demands and were also typical during the Vernalis Adaptive Management Plan (VAMP), which occurred from April 22 to May 22, 2008. Further, both water projects had similar pumping patterns from May 22, 2008 until early July 2008, when SWP pumping was conservative. Thus, the first simulation period—June 1 through July 12, 2008—represented typical low export conditions that occur during June. The average daily SWP export rate during the period used to calculate residence time in June 2008 was 19.3 $m^3 s^{-1}$ (689 cfs). Hydrological conditions in the Delta region were very dry between January and mid-February 2009, such that water exports in the Delta during the January through March 2009 period were restricted by the drier hydrological conditions earlier and the fisheries protections later (Le and Chu 2009). Thus, water exports during the second simulation period, from September 1, 2008 through April 30, 2009, were comparatively low relative to the historic mean for those months (Rossiter 2010). The average daily SWP export rate during the period used to calculate residence time in January 2009 averaged a moderate 66.6 $m^3 s^{-1}$ (2,351 cfs), whereas a typical high daily SWP export rate during winter months can exceed 170 $m^3 s^{-1}$ (6,000 cfs).

Model Formulation

The primary tool used in this technical study was the 3–D hydrodynamic model UnTRIM. A complete description of the governing equations, numerical discretization, and numerical properties of UnTRIM are described in Casulli (1999), Casulli and Walters (2000), and Casulli and Zanolli (2002, 2005).

The UnTRIM model solves the 3–D Reynolds-averaged Navier–Stokes equations (Equations 1 through 3) on an unstructured grid in the horizontal plane. The boundaries between vertical layers are at fixed elevations, and cell heights can be varied vertically to provide increased resolution near the surface or other vertical locations. Volume conservation is satisfied by a volume integration of the incompressible continuity equation (Equation 4), and the free-surface is calculated by integrating the continuity equation over the depth (Equation 5), and using a kinematic condition at the free-surface as described in Casulli (1990). The numerical method allows full wetting and drying of cells in the vertical and horizontal directions. The governing equations are discretized using a finite difference – finite volume algorithm. Discretization of the governing equations and model boundary conditions are presented in detail by Casulli and Zanolli (2002) and is not reproduced here. All details and numerical properties of this state-of-the-art 3–D model are well-documented in peer reviewed literature (Casulli and Zanolli 2002, 2005; Casulli 2009).

The UnTRIM model solves the full 3–D momentum equations for an incompressible fluid under a free-surface given by:

$$\frac{\partial u}{\partial t}+u\frac{\partial u}{\partial x}+v\frac{\partial u}{\partial y}+w\frac{\partial u}{\partial z}-fv=-\frac{\partial p}{\partial x}+\nu^h\left(\frac{\partial^2 u}{\partial x^2}+\frac{\partial^2 u}{\partial y^2}\right)+\frac{\partial}{\partial z}\left(\nu^v\frac{\partial u}{\partial z}\right) \tag{1}$$

$$\frac{\partial v}{\partial t}+u\frac{\partial v}{\partial x}+v\frac{\partial v}{\partial y}+w\frac{\partial v}{\partial z}+fu=-\frac{\partial p}{\partial y}+\nu^h\left(\frac{\partial^2 v}{\partial x^2}+\frac{\partial^2 v}{\partial y^2}\right)+\frac{\partial}{\partial z}\left(\nu^v\frac{\partial v}{\partial z}\right) \tag{2}$$

$$\frac{\partial w}{\partial t}+u\frac{\partial w}{\partial x}+v\frac{\partial w}{\partial y}+w\frac{\partial w}{\partial z}=-\frac{\partial p}{\partial z}+\nu^h\left(\frac{\partial^2 w}{\partial x^2}+\frac{\partial^2 w}{\partial y^2}\right)+\frac{\partial}{\partial z}\left(\nu^v\frac{\partial w}{\partial z}\right)-\frac{\rho}{\rho_0}g \tag{3}$$

where $u(x,y,z,t)$ and $v(x,y,z,t)$ are the velocity components in the horizontal x- and y-directions, respectively; $w(x,y,z,t)$ is the velocity component in the vertical z-direction; t is the time; $\rho(x,y,z,t)$ is the density; $p(x,y,z,t)$ is the normalized pressure defined as the pressure divided by a constant reference density, ρ_0 ; f is the Coriolis parameter; g is gravitational acceleration; and ν^h and ν^v are the coefficients of horizontal and vertical eddy viscosity, respectively (Casulli and Zanolli 2002). Conservation of volume is expressed by the continuity equation for incompressible fluids:

$$\frac{\partial u}{\partial x}+\frac{\partial v}{\partial y}+\frac{\partial w}{\partial z}=0. \tag{4}$$

The free-surface equation is obtained by integrating the continuity equation over depth and using a kinematic condition at the free-surface:

$$\frac{\partial \eta}{\partial t}+\frac{\partial}{\partial x}\left[\int_{-h}^{\eta}u\,dz\right]+\frac{\partial}{\partial y}\left[\int_{-h}^{\eta}v\,dz\right]=0 \tag{5}$$

where $h(x,y)$ is the prescribed bathymetry measured downward from the reference elevation and $\eta(x,y,t)$ is the free-surface elevation measured upward from the reference elevation (Casulli and Cheng 1992). Thus, the total water depth is given by $H(x,y,t)=h(x,y)+\eta(x,y,t)$. The National Geodetic Vertical Datum of 1929 (NGVD29) was used as the reference elevation.

The boundary conditions at the free-surface are specified by the prescribed wind stresses as:

$$\nu^v\frac{\partial u}{\partial z}=\tau_x^w,\qquad \nu^v\frac{\partial v}{\partial z}=\tau_y^w,\qquad \text{at}\ \ z=\eta \tag{6}$$

where $\tau_x{}^w$ and $\tau_y{}^w$ are the wind stress components in the x and y direction, respectively (Casulli and Zanolli 2002).

Similarly, at the sediment–water interface the bottom friction is specified by:

$$\nu^v\frac{\partial u}{\partial z}=\tau_x^b,\qquad \nu^v\frac{\partial v}{\partial z}=\tau_y^b,\qquad \text{at}\ \ z=-h \tag{7}$$

where $\tau_x{}^b$ and $\tau_y{}^b$ are the bottom stress components in the x and y direction, respectively. A quadratic stress formula is applied at each boundary. At the free-surface the coefficient of drag is specified as a function of wind speed using the formulation of Large and Pond (1981). At the bottom boundary the coefficient of drag is estimated using a specified roughness coefficient (z_0) following the approach described in MacWilliams (2004). The roughness coefficient z_0 was specified according to the elevation of each grid cell edge following the approach used by Cheng et al. (2003), Gross et al. (2010b) and MacWilliams et al. (2009) and ranged from 0.001 mm to 1.0 mm inside CCF, with higher roughness coefficient values specified in shallower areas.

The governing equation for salt transport (Casulli and Zanolli 2002) is:

$$\frac{\partial s}{\partial t}+\frac{\partial (us)}{\partial x}+\frac{\partial (vs)}{\partial y}+\frac{\partial (ws)}{\partial z}=\frac{\partial}{\partial x}\left(\varepsilon_h \frac{\partial s}{\partial x}\right)+\frac{\partial}{\partial y}\left(\varepsilon_h \frac{\partial s}{\partial y}\right)+\frac{\partial}{\partial z}\left(\varepsilon_v \frac{\partial s}{\partial z}\right) \quad (8)$$

where s is the salinity; ε_h is the horizontal diffusion coefficient; and ε_v is the vertical diffusion coefficient. The estimation of eddy viscosity and eddy diffusivity is discussed below. The system is closed by a linear equation of state of the form $\rho = \rho(s)$, which relates the water density to salinity.

The pressure in Equations 1 through 3 can be decomposed into the sum of its hydrostatic component and a nonhydrostatic component. The hydrostatic pressure component is determined from Equation 3 by neglecting the convective and the viscous acceleration terms. Thus, the normalized pressure can be expressed as:

$$p(x,y,z,t)=p_a(x,y,t)+g\left[\eta(x,y,t)-z\right]+g\int_z^{\eta}\frac{\rho-\rho_0}{\rho_0}d\zeta+q(x,y,z,t) \quad (9)$$

where $p_a(x,y,t)$ is the atmospheric pressure, the second and third terms on the right side of Equation 9 represent the barotropic and the baroclinic contributions to the hydrostatic pressure, and $q(x,y,z,t)$ denotes the normalized nonhydrostatic pressure component (Casulli and Zanolli 2002). For the simulations made in this study, the hydrostatic approximation was made and q=0 is assumed throughout.

A two-equation turbulence closure model comprised of a turbulent kinetic energy equation and a generic length-scale (GLS) equation is used to compute the distribution of vertical eddy viscosity in Equations 1 through 3. The parameters of the GLS equation are chosen to yield the "gen" closure proposed by Umlauf and Burchard (2003). The Kantha and Clayson quasi-equilibrium stability functions (Kantha and Clayson 1994) are used. This closure has been shown by Warner et al. (2005b) to have several advantages relative to the commonly used Mellor–Yamada level 2.5 closure, and to generally perform similarly to the GLS versions of k-ε and k-ω. All parameter values used in the "gen" closure are identical to those used by Warner et al. (2005b), including the minimum eddy diffusivity and vertical eddy viscosity values, which were 5 x 10^{-6} m^2 s^{-1}. The numerical method used to solve the equations of the turbulence closure is a semi-implicit method that results in tridiagonal positive-definite matrices in each water column and ensures that the turbulent variables remain positive (Deleersnijder et al. 1997). The effect of breaking wind waves on turbulence (e.g., Jones and Monismith 2008) is not accounted for in the turbulence closure. The horizontal eddy viscosity and eddy diffusivity were assumed to be zero, as in previous TRIM and UnTRIM applications (e.g., Gross et al. 2010b), because of the presence of numerical diffusion, which is at least on the order of physical horizontal turbulent diffusion in the numerical method of TRIM and UnTRIM.

FLEXIBLE INTEGRATION OF STAGGERED-GRID HYDRODYNAMICS PARTICLE TRACKING MODEL (FISH–PTM)

The Flexible Integration of Staggered-grid Hydrodynamics Particle Tracking Model (FISH–PTM) is a 3–D particle tracking model designed and developed to simulate particle trajectories using hydrodynamic model results from UnTRIM and other hydrodynamic models with similar grid structures. The theoretical aspects of particle tracking are discussed in detail by Dunsbergen (1994) and other sources.

The stochastic equation that describes particle transport is the Fokker–Planck equation (Dunsbergen 1994). The Lagrangian model that corresponds to the Fokker–Planck equation using the Itô integration rule can be written as

$$dX_i=\left[u_i+\frac{\partial D_i}{\partial x_i}\right]dt+R\sqrt{2r^{-1}D_i dt} \quad (10)$$

where i is the coordinate dimension, X_i is the particle position in the i dimension, u_i is the velocity in the i dimension, t is time, D_i is the diffusion coefficient in the i dimension, dt is the time step of integration, R is a realization of a uniformly distributed random number generator between −1 and 1, and $r = 1/3$ (Visser 1997; Stijnen et al. 2006). Isotropic horizontal diffusion $D_1 = D_2 = \varepsilon_h$ is assumed and the vertical diffusion $D_3 = \varepsilon_v$ is the eddy diffusivity estimated by the UnTRIM model.

The FISH-PTM solves Equation 10 in a manner that retains consistency with the numerical solution of the scalar (e.g., salinity) transport equation in UnTRIM (Equation 8) and several other hydrodynamic models. Additional details on the formulation of the FISH-PTM and test case results are provided by Gross et al. (2010a).

Model Input and Boundary Conditions

The UnTRIM CCF model was driven by inflows through the radial gates, exports at the Banks Pumping Plant, BBID exports, and wind forcing at the water surface. For each simulation the initial water level inside CCF was set to the observed water level inside CCF at the beginning of each simulation period. The bathymetric and model grid, and the implementation of the flow and wind boundary conditions, are described below.

Bathymetric and Model Grid

The California Department of Water Resources' North Central Region Office collected bathymetric data for CCF in December 2004 (Figure 2). The raw bathymetric soundings were converted to the NGVD29 vertical datum and interpolated onto a 10-m Digital Elevation Model (DEM). The bed elevation in the majority of CCF is between 1 and 3 m below 0 NGVD. Typical water levels inside CCF range from 0.5 m above 0 NGVD to as much as 1.0 m below NGVD. A scour hole more than 15-m deep is located immediately inside the radial gates, and the surrounding region inside the radial gates is quite shallow, with some shoals that are exposed when water levels inside CCF are below 0 NGVD. A deeper channel leads from CCF to the SFPF and Banks Pumping Plant.

A high resolution unstructured UnTRIM model grid was developed using the grid generator Janet (Lippert and Sellerhoff 2007). The UnTRIM CCF model grid consists of 17,817 elements, with the horizontal grid resolution ranging from 5 m near the radial gates to 40 to 50 m in the center of CCF (Figure 3). A vertical grid resolution of 10 cm was used, resulting in a total of more than 0.75 million computational prisms in 3–D. The CCF model used in this study has significantly increased grid resolution relative to the CCF grid included as part of the UnTRIM Bay–Delta model (MacWilliams et al. 2008, 2009) which consists of 2591 elements using a 1-m vertical resolution. The increased vertical grid resolution was necessary to resolve the surface layer effects from wind, and the increased horizontal resolution allowed for each of the five radial gates and the wing walls at the entrance to CCF to be resolved (Figure 3).

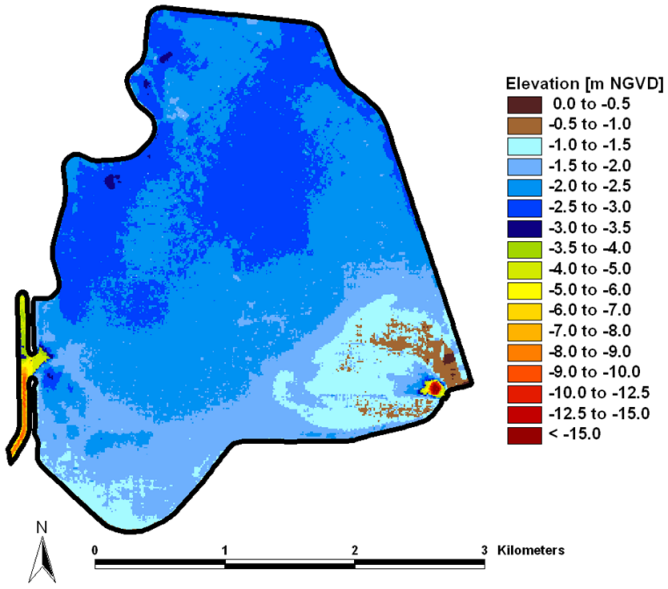

Figure 2 CCF bathymetry data collected in December 2004. Source: North Central Region Office, California Department of Water Resources.

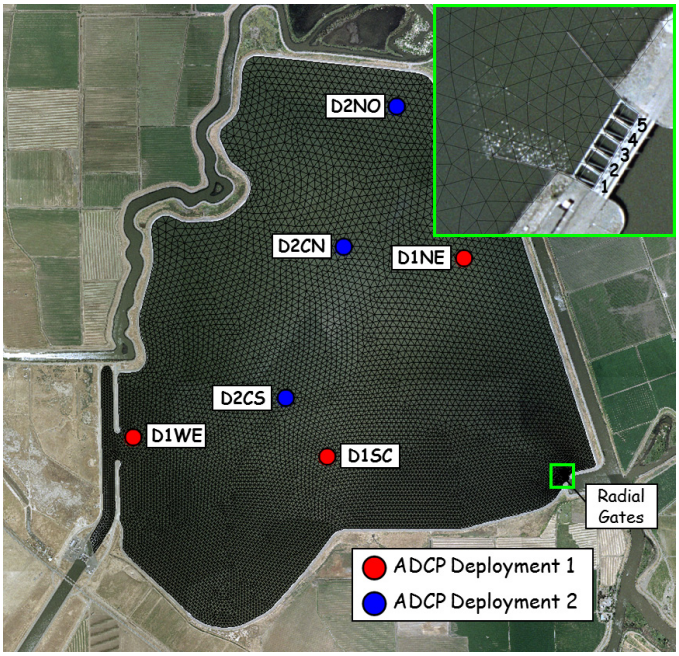

Figure 3 Location of upward-looking ADCPs during CCF data collection periods. ADCP Deployment 1 spans from September 19, 2008, to January 12, 2009 and ADCP Deployment 2 spans from January 13, 2009, to April 14, 2009.

Boundary Conditions

CCF acts as a regulating reservoir to moderate the effects of the SWP pumping on water levels in the Sacramento–San Joaquin Delta. Flow enters CCF through the radial gates, and is removed from CCF as exports from the Banks Pumping Plant, exports to the BBID, and through the net of evaporation and precipitation. The rate of change in volume inside CCF can be calculated as:

$$\frac{\Delta V_{CCF}(t)}{\Delta t} = Q_{RG}(t) - Q_{BANKS}(t) - Q_{BBID}(t) - Q_{EVAP-PRECIP}(t) \quad (11)$$

where V_{CCF} is the volume of water inside CCF, ΔV_{CCF} denotes the change in the volume of water inside CCF in the time increment Δt, Q_{RG} is the inflow through the radial gates, Q_{BANKS} is the exports at the Banks Pumping Plant, Q_{BBID} is the exports from CCF by the BBID, $Q_{EVAP-PRECIP}$ is the net evaporation of water from CCF, and t is time. By extension the rate of change in volume inside CCF is estimated by the observed change in water level:

$$\frac{\Delta V_{CCF}(t)}{\Delta t} = \frac{\Delta H_{CCF}(t)}{\Delta t} \times A_{CCF}(t, H) \quad (12)$$

where H_{CCF} is the average water surface elevation inside CCF, ΔH_{CCF} denotes the change of the average water surface elevation inside CCF in the time increment Δt, and A_{CCF} is the wet area inside CCF, which varies with water level. Since the average water surface elevation inside CCF cannot easily be measured, point elevations are typically substituted. However, a 0.03-m difference in water surface elevation changes the storage by 26,500 m^3 (21.5 ac-ft) and the inflow during a 15-min period by 29.4 $m^3\ s^{-1}$ (Hills 1988). As a result, the ability of the model to accurately predict water levels inside CCF over both short and long time scales is an indication that the inflows to CCF and the exports from CCF are being accounted for accurately and are consistent with the observed change in storage.

On a daily basis, the inflow to CCF is given by the reported DAYFLOW Q_{SWP} value (CDWR 1986). Note that the DAYFLOW formulation of Q_{SWP} has undergone several revisions, and that in previous versions of DAYFLOW Q_{SWP} was assigned the daily–average export rate from the Banks Pumping Plant (Tom et al. 2004). It is the authors' understanding that the daily Q_{SWP} values now being reported by DAYFLOW are derived from calculating the change in volume in CCF from the daily change in observed midnight water level inside CCF and then correcting for the Banks and BBID daily exports, such that

$$Q_{SWP}(t) = \frac{\Delta V_{CCF}(t)}{\Delta t} + Q_{BANKS}(t) + Q_{BBID}(t). \quad (13)$$

As such, Q_{SWP} represents the total daily inflow through the radial gates minus the daily net evaporation amount from CCF:

$$Q_{SWP}(t) = Q_{RG}(t) - Q_{EVAP-PRECIP}(t). \quad (14)$$

Since the net evaporation from CCF is already included in Q_{SWP} in Equation 14, applying additional evaporation or precipitation inside CCF was found to result in a deviation from observed water levels

over time. The only exception to this is on days when the radial gates do not open; then, Q_{SWP} is typically exactly zero. On days when Q_{SWP} is zero, evaporation from CCF should be applied separately to accurately maintain the water level inside CCF.

Daily and hourly values of exports from the Banks Pumping Plant are available in the DSS database (IEP 2010). Comparison between daily and hourly values indicate that pumping rates vary significantly across the day (pumping generally occurs at night when power is cheaper); however, daily–averaged hourly pumping data show some differences from the reported daily values. The volumes that result from the daily values were found to provide better agreement with observed water levels over extended periods of time. As a result, the hourly pumping values were normalized each day to match the reported total daily Banks Pumping Plant export volume. This approach was found to provide the best agreement between observed and predicted water levels inside CCF over both long and short time scales.

Daily values of BBID exports from CCF are available both from the DSS database (IEP 2010) and from the USBR daily "Delta Outflow Computation" data (USBR 2010). Daily BBID exports from the DSS database were applied in the UnTRIM model for this study.

Accurately estimating the timing and magnitude of inflows through the radial gates into CCF presents one of the biggest challenges to predicting water levels inside CCF and to accurately representing the influence of the SWP operations on Delta currents, water levels, and transport of biota (such as entrainment of fish into CCF). Various approaches have been used to estimate CCF inflows, and two new approaches were evaluated as part of this study.

Hourly flows through the radial gates can be estimated from the hourly water surface elevations inside and outside of CCF and the gate opening heights for each of the five CCF radial gates using the Hills (1988) gate equations:

$$Q_1 = H_1\left\{0.44 + 215.224\left(Elev_{outside} - Elev_{inside}\right)^{1/2}\right\} \quad (15)$$

$$Q_2 = H_2\left\{4.46 + 181.804\left(Elev_{outside} - Elev_{inside}\right)^{1/2}\right\} \quad (16)$$

$$Q_3 = H_3\left\{4.76 + 173.378\left(Elev_{outside} - Elev_{inside}\right)^{1/2}\right\} \quad (17)$$

$$Q_4 = H_4\left\{3.38 + 173.378\left(Elev_{outside} - Elev_{inside}\right)^{1/2}\right\} \quad (18)$$

$$Q_5 = H_5\left\{2.38 + 168.790\left(Elev_{outside} - Elev_{inside}\right)^{1/2}\right\} \quad (19)$$

$$Q_{RG} = Q_1 + Q_2 + Q_3 + Q_4 + Q_5 \quad (20)$$

where, Q_i is the flow through gate i (cfs), H_i is the gate opening height of gate i (ft), $Elev_{outside}$ is the water surface elevation outside of CCF (ft), $Elev_{inside}$ is the water surface elevation inside CCF (ft), and Q_{total} is the total CCF inflow through the radial gates (cfs). Le (2004) compared the flow through the radial gates calculated using the Hills (1988) equations to the inflow calculated by the California Department of Water Resources (CDWR) Delta Field Division from the actual measured storage in CCF (e.g., Equation 12) for two periods during 2002 and 2003. Le (2004) found that the inflow calculated using the Hills (1988) equations was similar to the inflow estimated by the change in storage during August and September 2003. On a monthly-averaged basis, Le (2004) also found that the Hills (1988) equations were within 6% of the monthly-averaged flow calculated from change in storage during April, July, September 2002 when exports were relatively high, but the estimates calculated using the Hills (1988) equations were 21% higher than the inflows calculated from the change in storage during May 2002 when both inflows to CCF and exports from CCF were relatively low.

Simulations made using the flows calculated using the Hills (1988) gate equations to calculate CCF inflows did not maintain accurate water levels inside CCF for the two periods simulated for this study. In order to obtain accurate mass conservation inside CCF, two new approaches for calculating the flow through the radial gates were evaluated. Using the first approach, referred to as the "normalized gate equations," gate flows into CCF calculated by the Hills (1988) equations were corrected to match the reported Q_{SWP} value for each day by multiplying them by the ratio of total daily reported volume to

total inflow volume calculated by the Hills (1988) equations. To use this approach, it is necessary to have hourly (or higher frequency) data for all five radial gate positions and observed water surface elevations inside and outside CCF, as well as the total daily inflow volume given by Q_{SWP}. Using the second approach, referred to as the "distributed SWP flow" approach, total Q_{SWP} flow was distributed uniformly over the time window on each day that the radial gates were open. For this approach, the only necessary information is the opening and closing times for the gates, and the total daily inflow volume given by Q_{SWP}.

Wind data from the closest available data station were used in each simulation. Wind data from a wind gauge at the radial gates were used for the simulation period from June 1 through July 12, 2008. For this period, hourly minimum wind speed, maximum wind speed, and average wind direction were available. The average of the hourly minimum and maximum wind speed was applied for this simulation period. Wind data from the Banks Pumping Plant were used for the simulation period from September 1, 2008, through April 30, 2009. Hourly average wind speed and direction were available for this simulation period. In each simulation spatially uniform wind was applied over CCF.

Observations Used in Calibration and Validation

Observed hourly water level data were available for the simulation period from June 1 through July 12, 2008 (IEP 2010). For the period from September 1, 2008, through April 30, 2009, only water level data at midnight were available. Comparisons between observed and predicted water levels were made using the highest frequency available observation data for each simulation period.

A series of velocity transects across the entrance channel to CCF outside of the radial gates were collected by the USGS to measure inflow through the radial gates on June 26 and June 27, 2008. The radial gates were opened three times during these 2 days. The measured flow across these transects was compared to flows calculated using each of the approaches evaluated for developing model boundary conditions for inflows into CCF.

The USGS deployed a total of seven upward-looking ADCPs in CCF between September 19, 2008, and April 14, 2009. The first deployment (D1) spanned from September 19, 2008, to January 12, 2009, and the second deployment (D2) from January 13, 2009, to April 14, 2009. During the first deployment, ADCPs were located at locations D1WE, D1SC, and D1NE (Figure 3). A fourth ADCP was deployed near the radial gates for part of this period; however, since data collected from the ADCP was not of sufficient quality to allow for meaningful comparisons to the model predictions, this station was not used in the analysis. During the second deployment, ADCPs were located at locations D2CS, D2CN, and D2NO shown in Figure 3. For each ADCP, predicted velocity was compared to the observed velocity over each ADCP bin at which valid data was collected.

The drifters used by the USGS in this study are similar in geometry to the TRISTAR drogue (Niiler et al. 1995), but are much smaller so that the USGS drifters can be used in shallow water. The drifters consist of a rod and flag that remain above water for visual location, a canister that is mostly underwater and houses electronics, a rigid tether, and a "kite" drogue similar to a TRISTAR drogue (Niiler et al. 1995) at the bottom of the tether. The rod that holds the flag is approximately 10 cm tall, and the flag is less than 5 cm tall and wide. The canister is 10 cm tall and 9 cm in diameter. When the drifter is deployed, the top of the kite is approximately 51 cm below the water line and the bottom of the kite is approximately 99 cm below the water line. The drogue consists of four triangular segments, each 48 cm from top to bottom, and 23 cm from the base to the tip of each segment.

A set of eight drifters was released in CCF at three different locations on June 26, 2008. The drifters remained in CCF until June 28, 2010, or until they reached the SFPF. The drifter deployments consisted of four groups each consisting of two drifters that were released at the same time and location. Because of vegetation inside CCF, the drifters were periodically retrieved and cleaned of weeds. Table 1 shows

relevant information about the deployment of each drifter, including the number of times and how long each drifter was immobilized ("stuck") during the deployment. Most of the drifters were stuck in vegetation or on the bed for a significant amount of time during the deployment, and the specific times that the drifters were immobilized often corresponded to relatively high water velocity periods, such as when the pumps were operating.

Model Evaluation Metrics

The quality of fit between predicted model results and observed time-series data is assessed following a cross-correlation procedure similar to that used by RMA (2005). This approach has also been used by MacWilliams and Gross (2007), MacWilliams et al. (2008, 2009), and Gross et al. (2010b), and provides a thorough description of the differences between time-series records through a quantitative measure of differences in terms of phase, mean, amplitude, and constant offsets. Statistics are derived to quantify the differences between predicted and observed time series data.

For the cross-correlation analysis, three different types of figures are shown. The top figure shows the tidal time scale variability for a period of approximately 15 days. On the bottom left, a daily-averaged plot for the full analysis period is shown. In previous studies, a tidal average was used; however, in CCF a daily average was found to be a more appropriate than a tidal average. On the lower right, the scatter plot shows a comparison between the observed and predicted data over the analysis period. The scatter plot is produced by first running a cross-correlation between the observed data and model predictions to find the average phase lag over the entire record. The cross-correlation was performed following the procedure outlined by RMA (2005). The process entails repeatedly shifting the predicted time-series record at 1-min increments relative to the observed time-series and computing the correlation coefficient at each time shift. The correlation has a maximum value when the shifted model time series best matches the observed time series. The time shift when the maximum correlation occurs represents the phase difference in minutes between the predicted and observed data, with positive values indicating that the predicted time series lags the observed time series. The linear regression is then performed between the time shifted model results and observed data record to yield the amplitude ratio, best-fit line, and correlation coefficient. The correlation coefficient (R), is a measure of the correlation between the model (*model*) and observations (*obs*):

$$R = \frac{\sum\left(X_{model} - \overline{X_{model}}\right)\left(X_{obs} - \overline{X_{obs}}\right)}{\left[\sum\left(X_{model} - \overline{X_{model}}\right)^2 \sum\left(X_{obs} - \overline{X_{obs}}\right)^2\right]^{1/2}} \quad (21)$$

where X is the variable being compared, and $\overline{X}$ is the time average of X. The value of the correlation

Table 1 Deployment information for USGS drifters deployed in CCF from June 26 to June 28, 2008

Drifter	X (m)	Y (m)	Release time	Recovery time	Times freed	Time stuck (hrs)
1	625547	4189296	6/26/08 09:10	6/28/08 09:43	2	4.58
2	625541	4189296	6/26/08 09:14	6/28/08 10:03	2	7.26
3	625549	4189296	6/26/08 09:35	6/28/08 08:07	4	9.52
4	625545	4189294	6/26/08 09:36	6/28/08 08:02	1	4.54
5	624206	4188533	6/26/08 08:58	6/26/08 12:08	1	0.67
6	624195	4188528	6/26/08 09:08	6/26/08 11:18	0	0
7	624918	4189291	6/26/08 09:00	6/28/08 11:12	12	12.66
8	624918	4189294	6/26/08 09:01	6/28/08 09:34	8	10.67

coefficient ranges from -1.0 (perfect negative correlation) to 1.0 (perfect positive correlation), with a value of 0.0 indicating no correlation. A perfect correlation occurs when all of the data points lie exactly on a straight line in a scatter plot of X_{obs} against X_{model}. For each time-series comparison, the correlation coefficient resulting from the cross-correlation analysis is reported.

An additional quantitative metric of model performance was used to compare between observed and predicted water level, velocity, and drifter velocities. Willmott (1981) defined the predictive skill based on the quantitative agreement between observations (*obs*) and model predictions (*model*) as:

$$Skill = 1 - \frac{\sum \left| X_{model} - X_{obs} \right|^2}{\sum \left(\left| X_{model} - \overline{X_{obs}} \right| + \left| X_{obs} - \overline{X_{obs}} \right| \right)^2} \quad (22)$$

where X is the variable being compared, and $\overline{X}$ is the time average of X. Perfect agreement between model results and observations yields a skill of 1.0. This metric of model skill has been used in a range of estuarine modeling studies (e.g., Warner et al. 2005a). Model skill was calculated for all comparisons between observed and predicted quantities.

RESULTS

The results of the CCF simulations are presented in this section. The CCF model was calibrated and validated through comparison to water levels, velocities, and drifter data. The model was then used to calculate residence time and travel time from the radial gates to the pumps.

Evaluation of Gate Equations

Initially, the Hills (1988) equations (Equations 15 through 20) were applied directly into the UnTRIM model to estimate inflows into CCF. However, the water levels inside CCF that were predicted using this approach consistently indicated that the Hills (1988) equations were overestimating flow through the radial gates. As a result, the USGS collected a series of velocity transects across the entrance of CCF to measure inflow through the radial gates on June 26 and 27, 2008. The radial gates were opened three times during these 2 days. On these 2 days, only radial gates 2, 3, and 4 were opened, and gates 1 and 5 were not used.

Figure 4 shows the operations target for flow through the radial gates, the measured flow through the radial gates, the flow through the radial gates predicted using the Hills (1988) equations, the normalized gate equations, and the distributed SWP flow. The CDWR Operations Branch provided the operator's real-time target for flow through the radial gates for these days. The USGS calculated measured flow by the using an autonomous boat to measure velocity along transects outside of the radial gates. The Hills (1988) gate equations were applied using the observed water levels inside and outside of CCF and the reported gate positions (IEP 2010).

Table 2 shows the reported total inflow volume and the daily average flow rate associated with each of these approaches for June 26 and 27, 2008. The measured inflow into CCF is within 0.66% of the Q_{SWP} value on June 26 and within 0.47% of the Q_{SWP} value on June 27. On both days, the measured flow is slightly higher than the reported value, which is consistent with the Q_{SWP} value being the total inflow minus the net evaporation (Equation 14). As shown

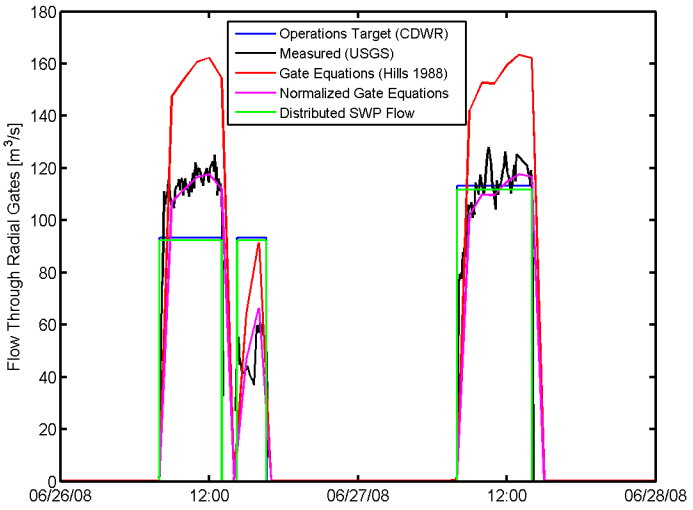

Figure 4 Flow estimates through the radial gates into CCF on June 26 and 27, 2008

in Figure 4, the Hills (1988) gate equations indicate significantly higher flow through the radial gates into CCF than observed. The predicted inflow using the Hills (1988) gate equations exceeds the reported Q_{SWP} value by 38.48% on June 26 and by 39.72% on June 27. Because the total daily inflow volume for the normalized gate equations and the distributed SWP flow is, by definition, set to be exactly the Q_{SWP} value, the percent error relative to Q_{SWP} is zero for both approaches as shown in Table 2.

As shown in Figure 4, the normalized gate equations approach is most similar to the measured flows on the 2 days for which data were collected. The distributed SWP flow approach is similar to the CDWR operations target flows on both days, and is similar to the observed flow on June 27, 2008. However, because the heights of the gate openings for the first and second times the radial gates were opened on June 26 were different, the distributed SWP flow approach, which assumes a daily uniform flow during the times that the gates are open, does not match the observed flow as closely on June 26. This result suggests that the normalized gate equations approach is preferable for periods when the necessary gate position and water level data are available; however, both approaches ensure the correct daily flow into CCF.

Simulations made using the Hills (1988) gate equations to calculate CCF inflows did not maintain accurate water levels inside CCF. UnTRIM simulations of CCF have been made using both the normalized gate equations and the distributed SWP flow approaches. The UnTRIM Bay–Delta model simulations used in the fish entrainment study by Gross et al. (2010a) were based on the UnTRIM Bay–Delta model implementation reported by MacWilliams et al. (2008), which used the normalized gate equations. This approach has been found to accurately predict water levels inside CCF for extended simulations. However, the implementation of this approach requires a priori knowledge of the water levels inside and outside CCF and the positions of the five gates. Data are available online for the period from September 9, 2000, through July 22, 2008 (IEP 2010), but have not been made available for either earlier or later periods. As a result, the distributed SWP flow approach has been used in simulations of earlier and later periods (i.e., MacWilliams et al. 2009). The distributed SWP flow approach also is more easily implemented for planning studies for future periods when the *a priori* water level data necessary for calculating the gate flows are not available. Both approaches have been found to meet the following multiple goals: to accurately predicting observed water levels inside CCF, to apply hourly operations to properly account for the effects of the radial gates on south Delta flows and water levels, and to maintain daily flow rates consistent with reported DAYFLOW values.

Model Calibration and Validation

Predicted water levels inside CCF were compared with observed hourly and daily water level data. Predicted velocities inside CCF were compared with velocity measurements collected from two separate

Table 2 Comparison of estimated inflow volume through the radial gates into CCF on June 26 and 27, 2008

Radial gate inflow calculation method	June 26, 2008			June 27, 2008		
	Total daily inflow volume (m^3)	Average flow rate ($m^3\ s^{-1}$)	Percent error relative to Q_{SWP}	Total daily inflow volume (m^3)	Average flow rate ($m^3\ s^{-1}$)	Percent error relative to Q_{SWP}
Q_{SWP}	2.4417×10^6	28.26	0.00	2.4148×10^6	27.95	0.00
Operations target (CDWR)	2.4726×10^6	28.62	1.27	2.4466×10^6	28.32	1.32
Measured (USGS)	2.4577×10^6	28.45	0.66	2.4262×10^6	28.08	0.47
Hills (1988) equations	3.3814×10^6	39.14	38.48	3.3728×10^6	39.05	39.72
Normalized gate equations	2.4417×10^6	28.26	0.00	2.4148×10^6	27.95	0.00
Distributed SWP flow	2.4417×10^6	28.26	0.00	2.4148×10^6	27.95	0.00

ADCP deployments. Comparisons were also made to drifter data collected inside CCF.

Water Surface Elevation

Figure 5A shows the observed and predicted water level inside CCF for the period from June 1, 2008, through July 10, 2008 for the simulation using the normalized gate equations. This period spans the time when the drifters were released in CCF. The top panel of Figure 5A shows the observed and predicted water level at the CDWR gauge located inside CCF near the radial gates for a 2-week period from June 25, 2008, to July 9, 2008. The predicted water levels are nearly identical to observed water levels from June 25 to 29, but show some differences in early July. The predicted daily average water level closely matches the observed daily average water level (lower left panel of Figure 5A), indicating that the total daily inflows and exports are being accounted for accurately. The mean predicted water level during this period is 1-cm higher than the mean observed water level, and the coefficient of determination (R^2) is 0.973. As seen in Table 3, the calculated model skill for the water level comparison for the period spanning from June 1 to July 11, 2008 is 0.991. A slightly lower skill of 0.989 for this same period is calculated for the corresponding simulation using the distributed SWP flow formulation for flow through the radial gates.

Figure 5B shows the observed and predicted midnight water level at the CDWR gauge located inside CCF near the radial gates for the period spanning from September 1, 2008 through May 1, 2009. The distributed SWP flow formulation for the radial gates was used for this period because hourly gate position data were not available. This period spans both ADCP deployments. Hourly water level data inside CCF were not available for this period, so only midnight values were compared. The mean observed and predicted water levels for this period are nearly identical, with a coefficient of determination (R^2) of 0.994 and a model skill of 0.998 (Table 3).

The accurate prediction of daily average water levels inside CCF (lower left panel of Figure 5A and left panel of Figure 5B) demonstrates that, on a daily basis, the inflows and exports from CCF are being accurately represented by the boundary conditions used in the UnTRIM CCF model for both the normalized gate equations and the distributed SWP flow formulations for flow through the radial gates are consistent with the observed change in storage. However, since the daily-averaged inflow reported in DAYFLOW is derived from the observed daily change in storage, these boundary values are not all independently measured. Conversely, the accurate prediction of instantaneous water levels inside CCF (top panel of Figure 5A) indicates that the use of inflows based on the normalized gate equations is accurately capturing the variability of water levels inside CCF over shorter time scales.

ADCP Velocity Comparisons

The upward-looking ADCPs deployed in CCF collected data averaged over discrete bins (either 1-m or 0.5-m thick). Because of the blanking distance above the instrument these ADCPs did not measure the velocity very near the bed. Similarly, surface velocities are not well resolved using 1-m vertical bins. As a result, the ADCP velocity comparisons only provide a measure of the model's ability to predict the sub-surface circulation patterns in CCF. For each comparison the observed and predicted u- and v-velocity components in each bin were plotted over a one week period. Since the model was forced with hourly data, both the observed and predicted velocities were filtered using a 4th-order Butterworth filter with a cutoff frequency of 1 hr^{-1} to remove higher frequency effects. A set of figures showing the observed and predicted velocity components at each ADCP location shown on Figure 3 is included in Appendix A. A 1-week period is shown in each comparison figure because the differences between observed and predicted velocity cannot be discerned from a plot of the full record. Table 3 provides the skill of the model in predicting the velocity at each station—both for the 1-week period shown in each figure included in Appendix A, and also for the full data record.

For the first deployment, a 1-week period from December 20 to 27, 2008 is shown in Appendix A The model skill also is evaluated for the data record

A

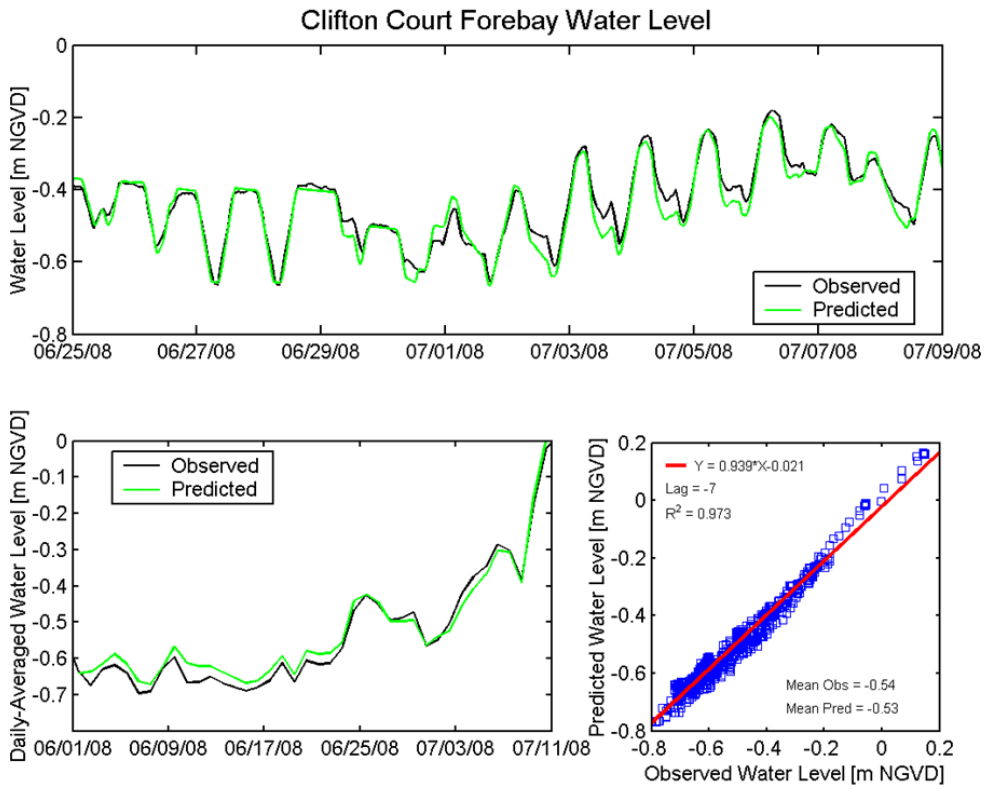

B

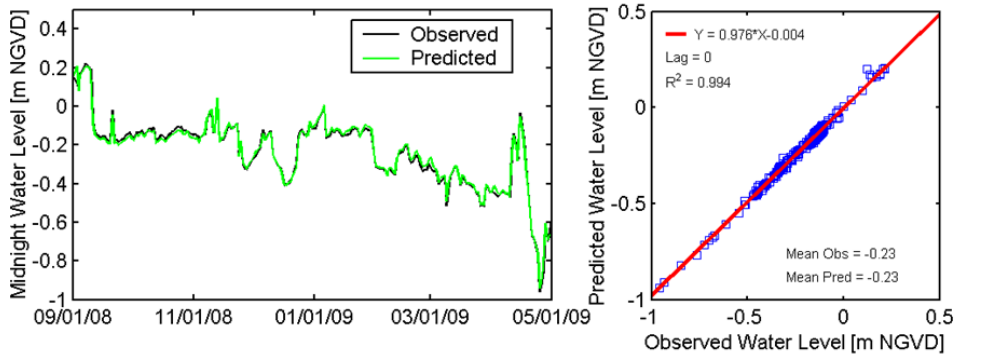

Figure 5 (A) Observed and predicted hourly (top) and daily-averaged (bottom left) water level inside CCF and cross-correlation statistics (bottom, right) during drifter and mark-recapture study of delta smelt (Castillo et al. 2012) for simulation spanning from June 1 to July 11, 2008; **(B)** Observed and predicted midnight water level inside CCF (left) and cross-correlation statistics (right) for simulation spanning from September 1, 2008, to May 1, 2009.

from October 29, 2008, to January 13, 2009. The period from September 19 to October 29, 2008, was not used in the analysis because hourly data for the Banks Pumping Plant were not available. Instead, daily data from Banks Pumping Plant were used in the model during this period. For the second deployment, a 1-week period from January 14 to 21, 2009 is shown in Appendix A. The model skill also is evaluated for the data record from January 13 to April 14, 2009.

Drifters

An ideal drifter would move at the water velocity in the drogue region of the drifter, corresponding to the "kite" located 0.51-m through 0.99-m below the water surface for the USGS drifters used in this study. However, drag is also exerted on other parts of the drifter. Wind drag acts directly on the rod, flag and the top of the canister. The portion of the canister in the water and the tether will be affected by drag force exerted by near surface currents (Geyer

Table 3 Skill scores from comparison of predicted and observed water levels and velocities

Water Level			
Data Frequency	**Radial Gate Implementation**	**Analysis Period**	**Skill**
Hourly	Normalized gate equations	6/01/2008 – 7/11/2008	0.991
Hourly	Distributed SWP flow	6/01/2008 – 7/11/2008	0.989
Daily (midnight)	Distributed SWP flow	9/01/2008 – 5/01/2009	0.998
Velocity			
ADCP Station	**Radial Gate Implementation**	**Analysis Period**	**Skill**
D1WE	Distributed SWP flow	10/29/2008 – 1/13/2009	0.94
		12/20/2008 – 12/27/2008	0.93
D1SC	Distributed SWP flow	10/29/2008 – 1/13/2009	0.75
		12/20/2008 – 12/27/2008	0.76
D1NE	Distributed SWP flow	10/29/2008 – 1/13/2009	0.67
		12/20/2008 – 12/27/2008	0.68
D2CS	Distributed SWP flow	1/13/2009 – 4/15/2009	0.65
		1/14/2009 – 1/21/2009	0.86
D2CN	Distributed SWP flow	1/13/2009 – 4/15/2009	0.48
		1/14/2009 – 1/21/2009	0.60
D2NO	Distributed SWP flow	1/13/2009 – 4/15/2009	0.46
		1/14/2009 – 1/21/2009	0.46

1989). Because the canister is near the water surface, the velocity around the canister will be more strongly influenced by wind, and the velocity in that layer will often be different from the velocity near the drogue. For this reason, the drifter will be more strongly influenced by wind than the "kite" drogue region alone. To account for this effect, the horizontal drifter velocity is typically estimated (e.g., Thompson et al. 2003) using the equation

$$u_{drifter} = u_{drogue} + \alpha u_{wind} \quad (23)$$

where $u_{drifter}$ is the drifter velocity u_{drogue} is the velocity at the drogue ("kite") portion of the drifter, α is the leeway factor, which can be estimated by analytical or empirical approaches (Thompson et al. 2003), and u_{wind} is the wind velocity 10-m above the water surface. Because most drifter studies have been in oceanic settings and used much larger drifters, and because the USGS drifters used in this study are not a standard design, simulations were conducted for several leeway factors, within the range of reported leeway factors in the literature, and a leeway factor of 0.006 was chosen for the drifter simulations. This value is similar to values in the literature for multiple drifter designs (Thompson et al. 2003) and consistent with the observed properties of the TRISTAR drifter studied by Niiler et al. (1995), which bears some similarity to the USGS drifter but is much larger.

The drifters released in CCF during the June 26 to 28 deployments were occasionally stuck on the bed or in vegetation. They were typically freed manually and released again. Table 1 shows the total time that each drifter was immobilized. To approximate the effect of the periodic immobilization of drifters on the bed and vegetation in the particle tracking simulations, during times when the drifter was immobilized the associated particle was also stopped and resumed moving only when the associated drifter was freed. For this reason, it is most appropriate to compare each drifter to a single associated particle. For example, drifter 1

and drifter 2 were released simultaneously in the same location. However, on June 16, 2008 at 17:06 PST, approximately 8 hrs after release, drifter 1 became stuck in vegetation for over 2 hrs while drifter 2 was still moving. Therefore, during the simulation the particle that represents drifter 1 was stopped from 17:06 to 19:17 PST while the particle that represents drifter 2 continued along its predicted trajectory at that time, causing the drifter and particle paths for drifter 1 and drifter 2 to diverge at this time.

In typical particle-tracking simulations, particles are allowed to move vertically in response to vertical velocities and turbulent mixing. However, the USGS drifters are designed to sample the velocity over a range of distance below the surface that corresponds to the location of the drogue "kite." For this reason, the particles in this simulation were specified to have the vertical location of the center of the drogue "kite," 0.76 m below the water surface. Given the vertical variability of velocity observed in the ADCP data and hydrodynamic model, the velocity over the "kite" could vary substantially. The wind observations used to specify u_{wind} in Equation 23 are the average of the minimum and maximum hourly wind observed at the CCF radial gates, which were also used in the hydrodynamic simulations. Horizontal

diffusion was neglected in the particle-tracking simulations. The CCF radial gate flows were estimated using the normalized gate equations approach.

The observed and predicted particle trajectories for each drifter are shown in Figure 6. The velocities that correspond to these trajectories were calculated by fitting a line to each observed and predicted trajectory over a 2.5-hr period. The observed and predicted velocities calculated for each drifter are shown in Appendix A and the corresponding model skill is reported in Table 4.

The predicted trajectories of drifters 1 through 4, which were released at approximately the same location near the center of CCF, do not extend as far west as the observed trajectories and therefore tend to be shorter (Figure 6A and 6B).

Drifters 5 and 6 (Figure 6C) were released at approximately the same location at the western end of CCF during a period of fairly calm winds and water exports from Banks Pumping Plant. Because of the strong effect of the exports on the observed and predicted trajectories, the direction of the predicted trajectories is very similar to the direction of the observed trajectories. However, the predicted trajectory for particle 5 is shorter than the observed trajectory of drifter 5. In contrast the length of the trajectory for drifter 6 is predicted accurately. One difference between drifter 5 and drifter 6 is that drifter 5 was affected by vegetation starting at 10:08 PST on June 26, 2008 and manually freed from vegetation at approximately 10:58 PST resulting in a later arrival at the channel leading to the Banks Pumping Plant than particle 6. Therefore, the comparison of observed and predicted trajectory for drifter 5 involves a longer period, relative to drifter 6, and includes a period when the particle is "stuck."

The predicted trajectories of drifters 7 and 8 (Figure 6D), which were released in approximately the same location west of the center of CCF, do not extend as far east as the observed trajectories. The predicted trajectories for these particles were sensitive to the specified leeway factor because the wind velocity and the water velocity acting on the drogue were in different, roughly opposing, directions during much of the simulation period. An increased leeway factor of 0.008 improved the predictions in the later, strong wind period for these two drifters, but decreased the accuracy of the trajectory predictions for other drifters.

For comparison, the hydrodynamic and particle-tracking scenarios of the drifter releases were repeating using the distributed SWP flow approach to estimate CCF radial gate flows. The trajectories and corresponding model skill estimated in those simulations (Table 4) were generally similar to the results for the normalized gate equations, discussed earlier.

Transport Time Scale Estimates

Two complementary transport time scales were estimated by particle tracking simulations in CCF. These time scale estimates were provided for periods of low-export and moderate-export pumping conditions,

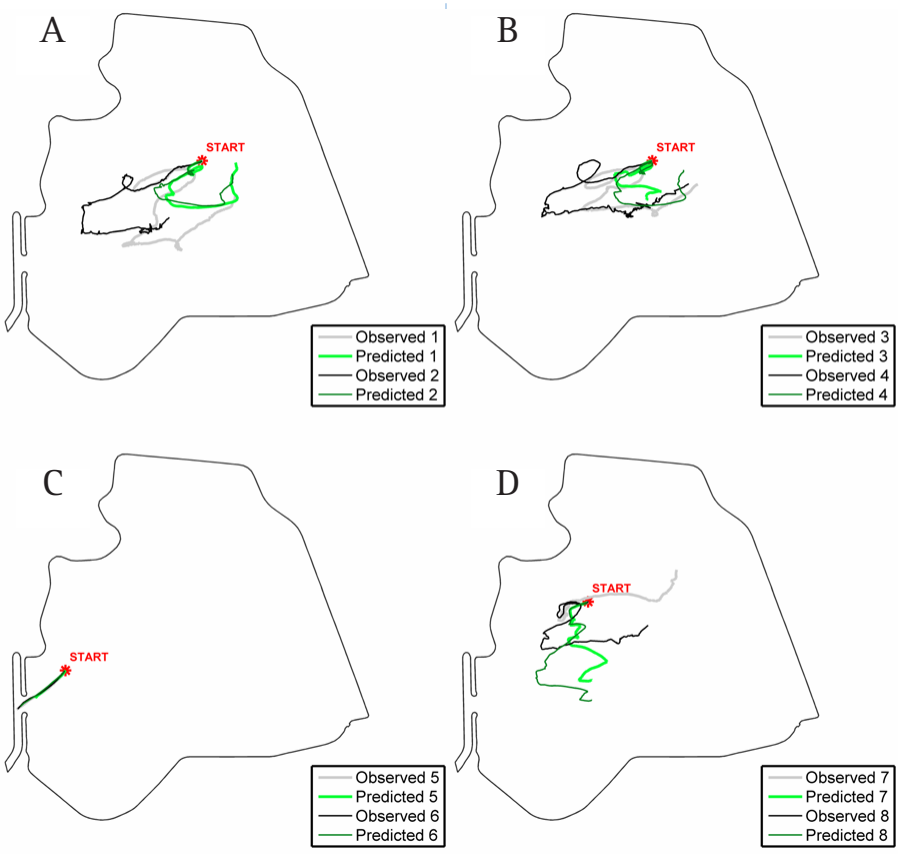

Figure 6 Observed and predicted drifter trajectories from the USGS field study in CCF conducted from June 26 to 28, 2008: **(A)** drifters 1 and 2; **(B)** drifters 3 and 4; **(C)** drifters 5 and 6; **(D)** drifters 7 and 8

which should be useful in the interpretation of salvage data collected at the SFPF.

Residence Time

Residence time is defined by Monsen et al. (2002) as the time that "a parcel, starting from a specified location within a waterbody, will remain in the waterbody before exiting." To estimate the range of residence time in CCF, particle-tracking simulations were conducted for both low export pumping conditions and moderate export pumping conditions. The release time for low pumping conditions was June 9, 2008 and the release time for moderate pumping conditions was January 10, 2009. In each simulation particles were released at mid water column distributed on a uniform grid across CCF with a horizontal spacing of 50 m. We chose a 21-d simulation period because that was approximately the period of continuous low exports beginning on June 9, 2008. Each particle was tracked for the lesser of 21 d, and the time to entrainment by the pumps. For each entrained particle, the residence time was then calculated as the time of entrainment minus the particle release time.

Unlike the particle-tracking simulations of drifter observations, which represented the predicted trajectory of drifters with a fixed vertical position, the particles in the residence time simulation were allowed to mix in the vertical according to the turbulence properties estimated by the UnTRIM model. As in the drifter observation comparison simulations, horizontal diffusion was neglected in these simulations. In sensitivity simulations, inclusion of horizontal diffusion had a small effect on the residence time.

Table 4 Skill scores from comparison of predicted particle velocity with observed drifter velocity

Drifter	Radial gate implementation	Skill
1	Normalized gate equations	0.699
	Distributed SWP flows	0.688
2	Normalized gate equations	0.810
	Distributed SWP flows	0.808
3	Normalized gate equations	0.589
	Distributed SWP flows	0.556
4	Normalized gate equations	0.795
	Distributed SWP flows	0.766
5	Normalized gate equations	0.191
	Distributed SWP flows	0.163
6	Normalized gate equations	0.494
	Distributed SWP flows	0.431
7	Normalized gate equations	0.558
	Distributed SWP flows	0.572
8	Normalized gate equations	0.870
	Distributed SWP flows	0.868

The calculated residence times for the two simulations are shown in Figure 7. A large range of residence time was estimated for the release on June 9, 2008, which occurred during low export flow conditions. The trajectories of two particles released on June 9, 2008, near the radial gates, are shown in Figure 8A. One particle rapidly crossed CCF and was entrained, while the other looped around CCF several times, according to wind circulation patterns. The average residence time for the low pumping conditions particle release was 8.8 d and 3.6% of the particles were not entrained after 21 d. In contrast, most of the particles in the release on January 10, 2009, during moderate export flow conditions, have relatively short residence times, and the estimated residence times are strongly correlated with distance from the Banks Pumping Plant water exports. The trajectories of two particles released on January 10, 2009, near the radial gates, are shown in Figure 8B. Both particles crossed CCF without significant recirculation inside CCF. One particle took a curved path, while the other took a more direct path to the Banks Pumping Plant. The average residence time

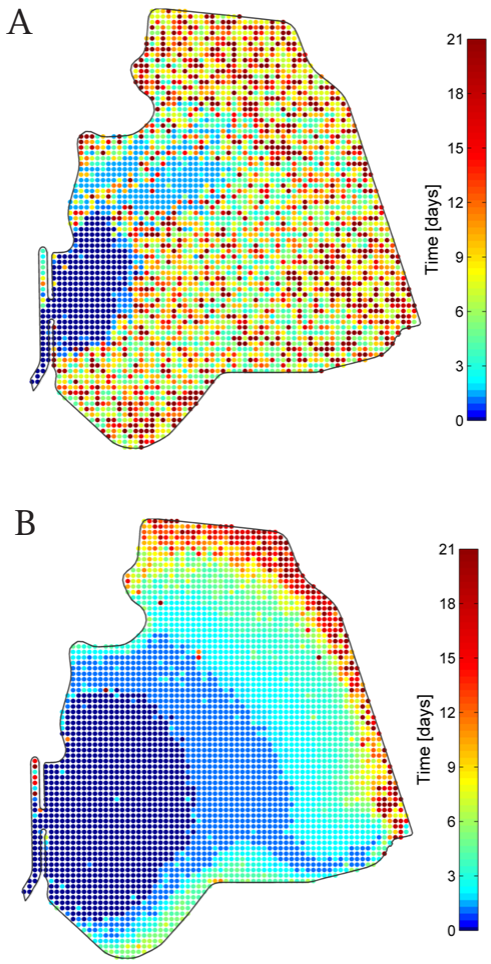

Figure 7 Predicted residence time of particles shown at the release location of each particle. **(A)** Particles released on June 9, 2008 at 00:00 PST during low export pumping conditions; **(B)** Particles released on January 10, 2009 at 00:00 PST during moderate export pumping conditions.

during the moderate export flow conditions particle release was 3.0 d, and 2.0% of the particles were not entrained after 21 d.

Transit Time and Age

An additional set of simulations was conducted to estimate transport time scales in CCF during the same periods used in the residence time analysis. In these simulations, particles were released at the radial gates. The number of particles released was proportional to the instantaneous flow through the radial gates with each particle representing a volume

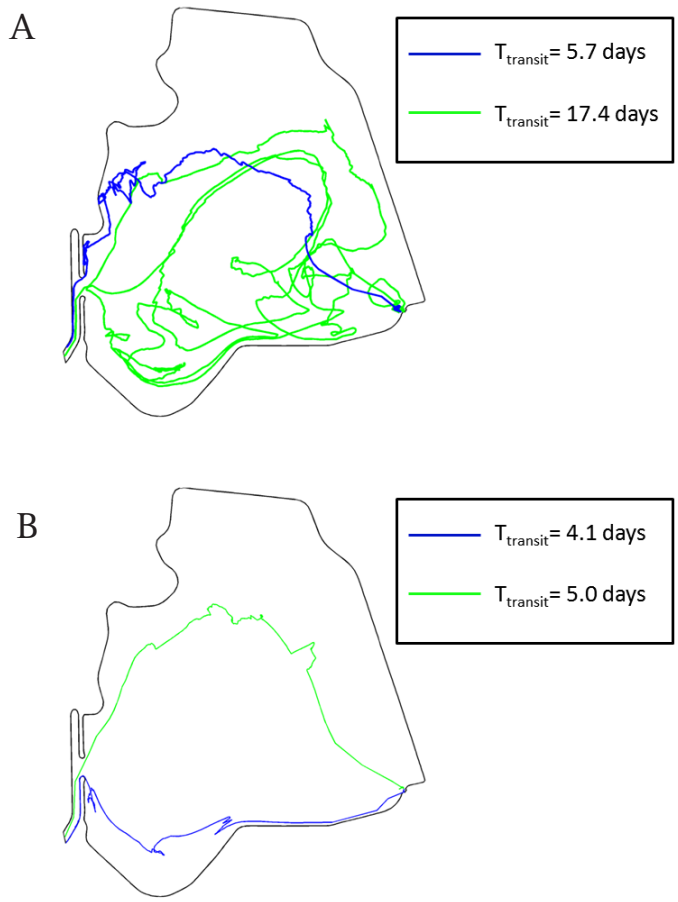

Figure 8 Predicted trajectories for two different particles released near the radial gates. **(A)** Particles released on June 9, 2008 at 00:00 PST during low export pumping conditions; **(B)** Particles released on January 10, 2009 at 00:00 PST during moderate export pumping conditions.

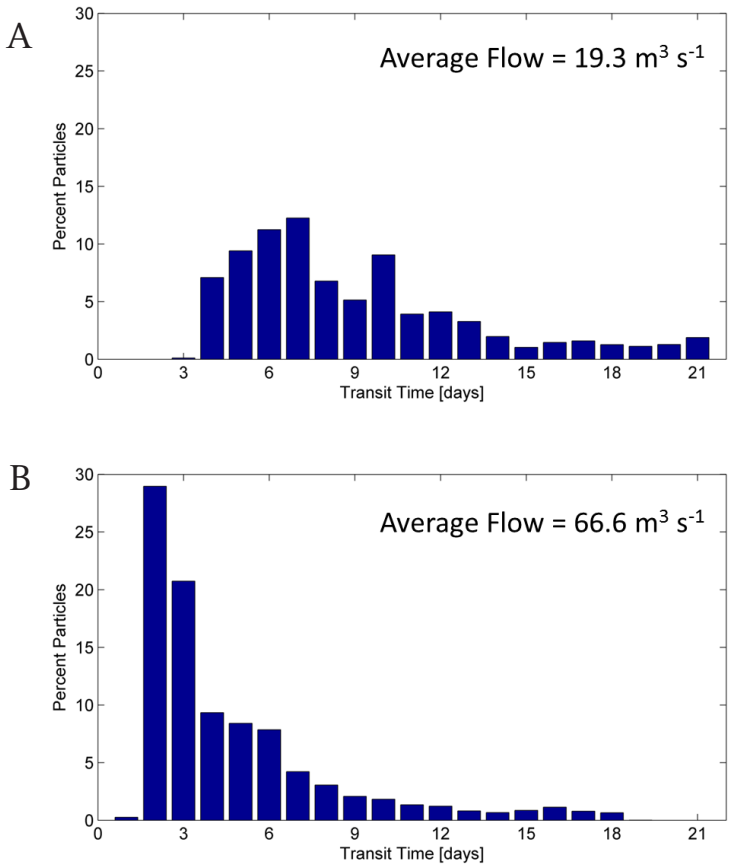

Figure 9 Predicted transit time of particles from the Clifton Court Forebay radial gates to the SWP exports. **(A)** Particles released on June 9, 2008, during low export pumping conditions; **(B)** Particles released on January 10, 2009, during moderate export pumping conditions.

of 1,000 m^3 of water. Each particle was then tracked for 21 d or until entrained at the SFPF. From these results, two different transport time scales were estimated. The first was the residence time of particles released at the radial gates in CCF, which we will refer to as "transit time." The second is the "age" of particles, which is the time elapsed since a particle (water parcel) at a particular location has entered the domain (Monsen et al. 2002).

The estimated transit times for particles that entered CCF on June 9, 2008, and particles that entered CCF on January 10, 2009, are shown in Figure 9. The average transit time of particles that enter on June 9, 2008 that were entrained during the simulation was 9.1 d, and 16.0% of the particles were not entrained at the end of the 21-d period. In contrast, the average transit time of particles that enter on January 10, 2009 that were entrained during the simulation was 4.8 d, and only 5.0% of particles were not entrained at the end of the 21-d period.

At any moment in time during these simulations, each particle in CCF has an age, which is the time elapsed since the particle entered CCF. For the transit time results shown, only particles that entered CCF on June 9, 2008 and on January 10, 2009 were considered. In contrast, for the age calculations, all particles that entered CCF during the simulation

period were considered, not just particles that entered on June 9, 2008 or January 10, 2009. After 21 d of particle-tracking simulation, the age of all particles present in CCF for each period is shown in Figure 10. The age of particles is generally much lower for the moderate export flow period, and the particles with the highest age are located in the northern portion of CCF. During moderate export flow conditions, only the far northern portion of CCF contains a substantial number of particles with ages older than 10 d.

DISCUSSION

Circulation Patterns in Clifton Court Forebay

Circulation patterns in CCF are largely driven by: (1) wind on the surface of CCF, (2) the operation of the radial gates, which allow inflow to CFF, and (3) the operation of the Banks Pumping Plant, which exports water from CCF. To understand how wind and operations influence circulation in CCF, predicted surface and subsurface currents in CCF are compared during periods with high and low winds, and during periods with and without operation of the radial gates and the Banks Pumping Plant.

Figure 11 shows the predicted circulation patterns in CCF for two times during periods of high sustained winds. On June 25, 2008 at 00:00 PST, a period of relatively high average wind speeds, when the radial gates are closed and the Banks Pumping Plant is not operating (Figure 11B), surface currents exceeded 0.20 m s^{-1} in most of CCF, with a predominant direction from southwest to northeast. The wind forcing at the surface sets up a large counter-clockwise subsurface circulation cell, which runs north along the eastern edge of CCF. Predicted subsurface current speeds exceed 0.10 m s^{-1} along the eastern and southern portions of this circulation cell. The high-velocity region along the eastern side of CCF corresponds to the deeper region along the eastern edge of CCF shown in Figure 2. Several smaller circulation cells are evident in the northern part of CCF. On June 24, 2008 at 16:00 PST, a period of relatively high average winds speeds, when the radial gates are open and the Banks Pumping Plant is operating (Figure 11C), the surface currents show a strong wind forcing as they did in Figure 11B, but are somewhat lower than

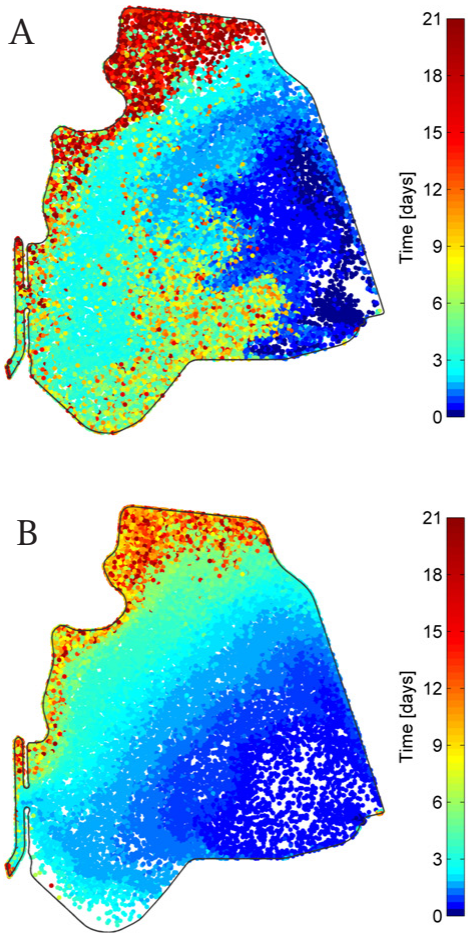

Figure 10 Predicted age of particles that enter through the radial gates shown at the location of each particle at the end of the simulation period. **(A)** Particles released from June 9, 2008 through June 29, 2008 during low export pumping conditions; **(B)** Particles released from January 10, 2009 through January 30, 2009 during moderate export pumping conditions.

the surface currents on Figure 11B; this difference appears to be largely because the high wind period is just beginning, as seen in Figure 11A. Surface current speeds exceeded 0.20 m s^{-1} near the radial gates but are deflected to the northeast by the surface winds. Subsurface currents are somewhat less strong than in those in Figure 11B, however the primary subsurface flow path from the radial gates to the Banks Pumping Plant is the counterclockwise gyre along the eastern edge of CCF and then west across the northern portion of CCF. The southern portion of the counterclockwise gyre seen on Figure 11B is not evident on Figure 11C, since the subsurface flow is being

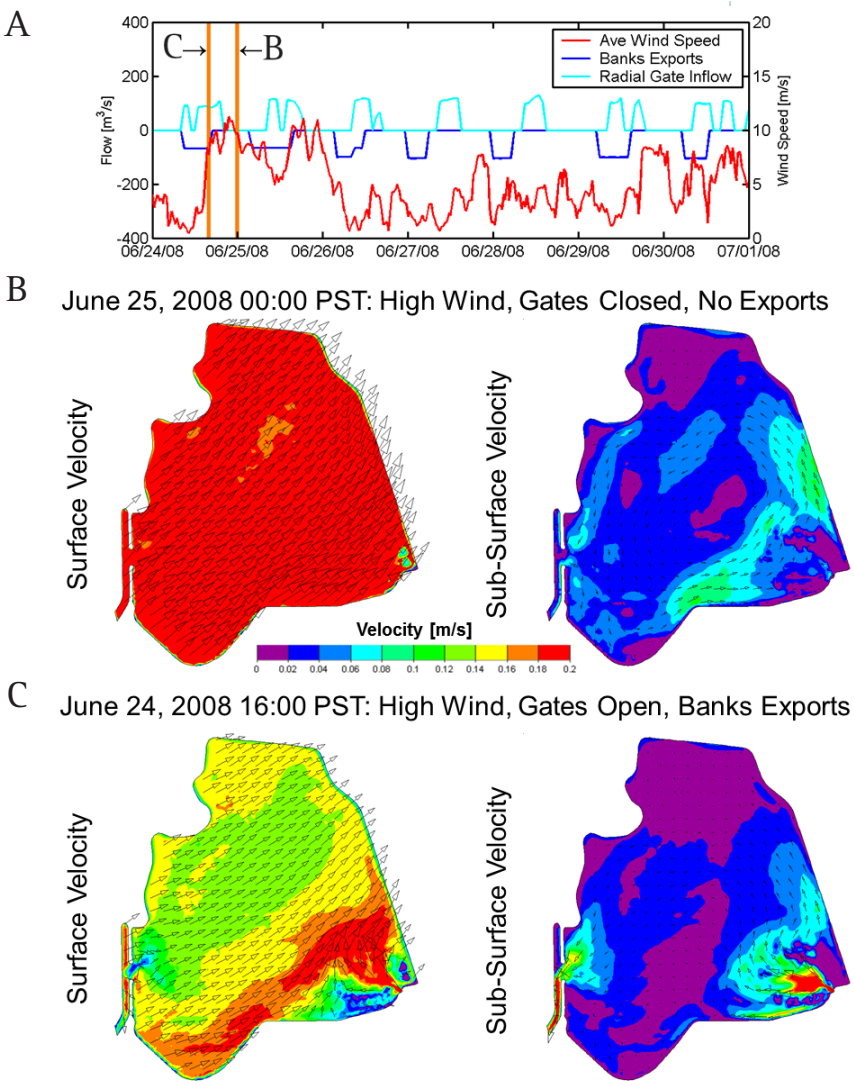

Figure 11 **(A)** Flow through the radial gates, exports at the Banks Pumping Plant, and average observed wind speed from June 24, 2008, to July 1, 2008; **(B)** Predicted surface and subsurface circulation patterns in CCF on June 25, 2008 at 00:00 PST, during a period with relatively high winds, when the radial gates were closed and the Banks Pumping Plant was not operating (time indicated by orange line marked "B" in panel A); **(C)** Predicted surface and subsurface circulation patterns in CCF on June 24, 2008 at 16:00 PST, during a period of relatively high winds, when the radial gates were open and the Banks Pumping Plant was operating (time indicated by orange line marked "C" in panel A).

entrained into the channel on the west side of CCF leading to the Banks Pumping Plant.

In contrast to the circulation patterns on June 24 and June 25 during a period of relatively high wind speeds, Figure 12 shows the predicted circulation patterns in CCF for two times during periods with low wind speeds. Figure 12B shows the predicted circulation patterns in CCF on January 14, 2009 at 22:00 PST, a period of very low average wind speeds, when the radial gates were closed and the Banks Pumping Plant was not operating. Surface currents and subsurface currents are less than 0.02 m s^{-1} throughout CCF. Some small subsurface circulation gyres are still present but the strength of these circulation cells is less than 10% of the strength of the circulation gyres evident on June 25, 2008 at 00:00 PST. Figure 12C shows the predicted circulation patterns in CCF on January 15, 2009 at 01:00 PST, a period of relatively low average wind speeds, when the radial gates were open and the Banks Pumping Plant was operating. Inflow rates through the radial gates and export flow rates at the Banks Pumping Plant on January 15, 2009 were approximately twice as large as those on June 24 to 25, 2008. Surface current speeds exceed 0.20 m s^{-1} near the radial gates and in the channel that leads to the Banks Pumping Plant. Subsurface currents exhibit a similar pattern to the surface currents, with strong west-to-east flow throughout most of CCF. The predominant flow pathway under these conditions, both on the surface and below the surface, is due west from the radial gates towards the Banks Pumping Plant. The subsurface counter-clockwise gyre seen in Figure 11 was not present under low wind conditions when the radial gates were open and the Banks Pumping Plant was operating.

The predicted circulation patterns shown in Figures 11 and 12 provide some insight into the transport time scale results for summer low export flow conditions. The residence

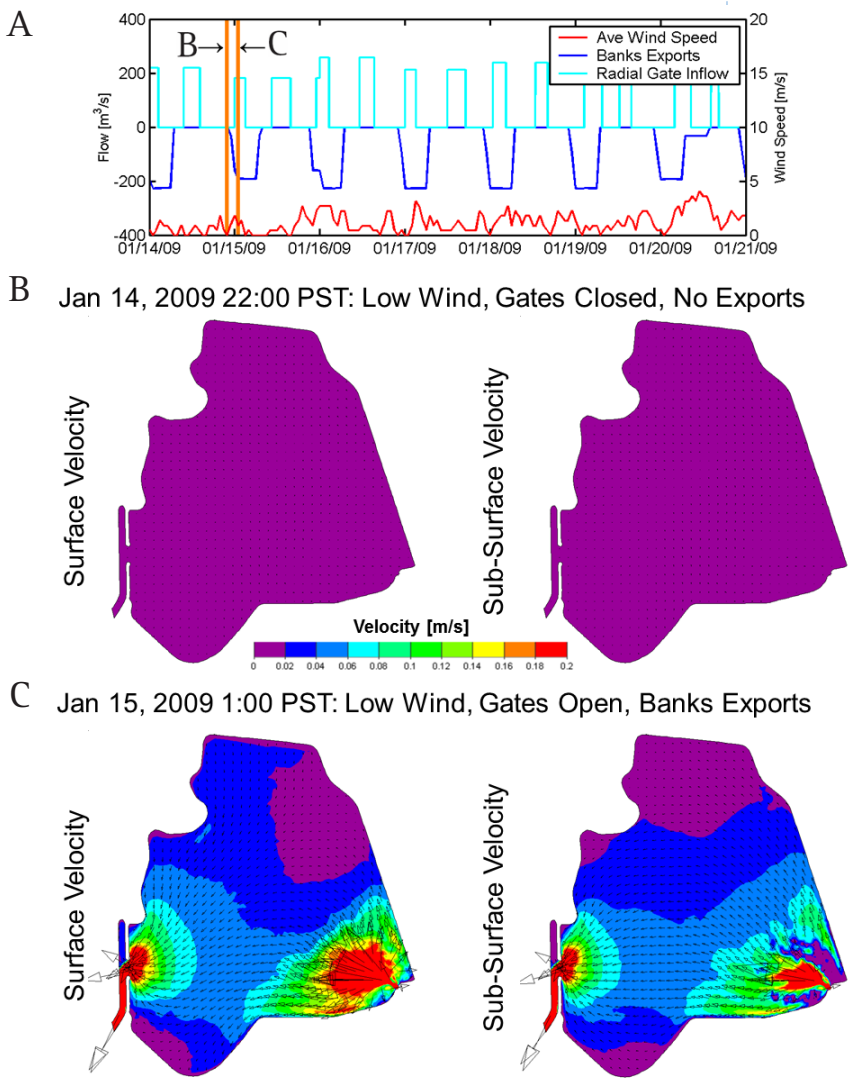

Figure 12 **(A)** Flow through the radial gates, exports at the Banks Pumping Plant, and average observed wind speed from January 14, 2009 to January 21, 2009; **(B)** Predicted surface and subsurface circulation patterns in CCF on January 14, 2009 at 22:00 PST, during a period with very low winds, when the radial gates were closed and the Banks Pumping Plant was not operating (time indicated by orange line marked "B" in panel A); **(C)** Predicted surface and subsurface circulation patterns in CCF on January 15, 2009 at 1:00 PST, during a period of relatively low winds, when the radial gates were open and the Banks Pumping Plant was operating (time indicated by orange line marked "C" in panel A).

time estimates during summer conditions (Figure 7A) exhibit some chaotic behavior with estimated residence time for adjacent particle releases typically varying greatly. This result is largely explained by the variability between surface velocities and subsurface velocities shown in Figure 11. Because the particles are being mixed vertically by turbulence in a random manner, each particle will be at the surface during different periods, resulting in wide variability in particle trajectories. For this reason, a large range of transit time is predicted during summer (Figure 9A). Some small scale spatial variability is evident in the age estimates and the age distribution suggests that the most common trajectory followed by particles that enter the radial gates is to move north along the eastern shore of CCF and then southwest toward the Banks Pumping Plant.

The predicted circulation patterns shown in Figure 12 provide some insight to the transport time scale results for the winter higher export flow conditions during a period of relative calm wind. The residence time estimates during winter conditions (Figure 7B) increase from west to east and are largest along the eastern and northern shoreline. The less chaotic variability of the residence time estimates, relative to the summer condition estimates, can be understood by the similarity in direction of surface and subsurface velocities, which are from the radial gates toward the Banks Pumping Plant (Figure 12C). Therefore the direction of a particle trajectory will not change substantially with vertical position during these conditions. A smaller range of transit time and lower average transit time is predicted during winter conditions (Figure 9B) relative to summer conditions (Figure 9A) because of higher pumping and a less pronounced effect of wind. The age distribution suggests that the majority of particles that enter at the radial gates

move directly toward the Banks Pumping Plant. The particles that follow a trajectory to the north of CCF can reach a relatively large age, which is consistent with the low velocities in the north of CCF indicated in Figure 12.

In the comparison between observed and predicted velocities, the predicted velocity at several stations in the northern part of CCF is less than the observed velocity and has much less variability on short time scales. As seen in Figure 11, the northern portion of CCF is outside of the large subsurface circulation gyre. In this region, several smaller and weaker circulation gyres are predicted. This complexity in circulation pattern may account for the lower model skill in the comparisons at stations D2NO and D2CN (Table 3) since small shifts in the locations of these gyres could result in a noticeably different velocity. However, some of the differences between observed and predicted velocities are also likely the result of using spatially uniform hourly average wind data, which is not likely to capture all of the spatial and temporal wind variability that drives circulation in CCF.

Gate Equations

Based on the data reported by Hills (1988), a total of 12 flow measurements at each gate were used to develop the gate equations. These 12 measurements all correspond to relatively large gate opening heights, mostly 4.3 m or 4.6 m (14 ft or 15 ft). Only one of the twelve measurements used was made when the gate opening heights were set for either 3.0 m or 3.7 m (10 ft or 12 ft). Hills (1988) reported five other flow measurements were made with gate openings between 3.0 m and 3.7 m (10 ft and 12 ft), but these measurements were not used in determining the flow equations for the gates. Thus the Hills (1988) equations were calibrated mostly for gate opening heights in the 4.3 m to 4.6 m (14 ft to 15 ft) range. However, under current operations during periods such as VAMP when the inflows to CCF are relatively low, the radial gates are typically opened less than 3.0 m (10 ft). On June 26, 2008 (Figure 4) radial gates 2 through 4 were opened at a height of 1.8 m (5.8 ft) between 9:00 and 13:00 PST, and were opened at heights of between 0.9 m and 1.5 m (3.0 ft and 5.0 ft) between 15:00 and 16:00 PST. Flow measurements collected near the radial gates for 2 days during relatively low inflows (Figure 4) suggest that the Hills (1988) gate equations are not accurate under these conditions. The Hills (1988) gate equations overestimate inflow on June 26, 2008 by 38.48%, and over-estimate inflow on June 27, 2008 by 39.72% (Table 2).

This result is consistent with the findings of Le (2004), which indicated that the largest difference between the inflows calculated using the Hills (1988) equations and the inflows calculated from the change in storage were greatest during periods when both inflows to CCF and exports from CCF were relatively low. During May 2002, when Le (2004) reported that the monthly-averaged inflow to CCF calculated using the Hills (1988) equations was 21% higher than the inflow estimate derived from the change in storage, the monthly-averaged measured inflow through the CCF gates was only 19.2 $m^3 s^{-1}$ (678 cfs), which is nearly identical to the average export rate of 19.3 $m^3 s^{-1}$ during the 21-d period in June 2008 that was used to compute residence time in this study. A similar over-estimate of inflow calculated using the Hills (1988) equations is evident on June 26 and 27, 2008 (Figure 4). One likely explanation for the over-estimate of inflows calculated using the Hills (1988) equations during these two days is that when the gates are not fully opened the flow through the gates on the downstream side is “fully submerged” creating an orifice-type flow condition (Clemmens et al. 2003). However the data used in calibrating the Hills (1988) equations were collected mostly under partially-submerged conditions. A gate flow equation calibrated for partially submerged conditions will ordinarily overpredict the flow rate through the gate if it is used for fully submerged conditions.

Additionally, the Hills (1988) gate equations were calibrated under conditions when all five CCF radial gates were opened and closed in unison. As noted by Hills (1988), flows through gate 1 (the southernmost gate) is greater than the other gates with the same openings, which indicates there is an effect on the individual gate calibrations from the non-uniform velocity distribution in the approach cross-section to the gates. On June 26 and 27, 2008, only radial gates

2 through 4 were opened and gates 1 and 5 remained closed. Thus, additional calibration of the gate equations also may be required for periods when the five gates do not all operate in unison.

Additional data should be collected for a wider range of operating conditions, and recalibrated gate equations should be developed to improve the accuracy of inflow predictions. In addition, the increased availability of hourly (or higher frequency) data on elevations inside and outside CCF as well as detailed information on the five gate positions would allow for further analysis of flows into CCF under a wider range of operating conditions, and allow for the application of the normalized gate equations approach (Figure 4) which will allow for improved entrainment estimates for simulations of historic periods.

This analysis indicates that the radial gates are currently being operated at opening heights that are well outside of the height ranges for which the Hills (1988) equations were calibrated, and suggests that recalibration of the gate equations may be needed for periods when the gates are not fully opened (such as for VAMP) or when all five gates are not operated in unison. The differences in daily flow into CCF during the VAMP period are particularly important for entrainment studies, since these periods are critical periods for delta smelt entrainment at the SWP.

CONCLUSIONS

The results presented in this paper constitute the first detailed analysis of circulation and residence time inside CCF. The predicted water levels agree extremely well with observed water levels. These results demonstrate that the model accurately accounts for the volume and timing of inflows to and exports from CCF on both hourly and daily time–scales. Accurately predicting the timing and magnitude of inflows into CCF is essential for studies that evaluate how operations affect entrainment.

An evaluation of the Hills (1988) gate equations indicates that the gate equations result in significant variances in inflow from the observed values, particularly during periods when inflows are small. Flow measurements collected near the radial gates for 2 days during relatively low inflows suggest that the Hills (1988) gate equations may overestimate inflow by approximately 39%. These periods with low inflows to CCF typically correspond to periods when entrainment is a significant concern. Two different approaches presented in this paper were both shown to produce accurate daily inflows for the periods evaluated. For historic periods, when the five gate positions and observed inside and outside water levels are available, the normalized gate equations approach produces the most accurate results for the periods evaluated. For the longer historical record when these data are not available, or for planning studies, the distributed SWP flow approach can be applied provided that the daily SWP flow and gate opening and closing times are known.

The comparisons of predicted velocity to measured velocity indicate that the model is capturing many of the large-scale circulation features inside CCF, particularly during periods when the circulation is dominated by inflow and export operations. However, the predicted velocity at several stations in the northern part of CCF is less than the observed velocity and shows much less variability on short time scales. This suggests that forcing the model using spatially uniform, hourly-averaged wind data may not be adequate to capture all of the flow complexity in this portion of CCF. Wind waves may also play an important role in circulation and mixing in this region. It is likely that circulation predictions could be somewhat improved by first collecting higher frequency wind observations for surface boundary conditions, and then simulating wind waves and parameterizing the effect of breaking wind waves on vertical turbulent mixing. Collection of ADCP observations with more vertical bins would allow more detailed calibration of model results.

Predicted drifter trajectories are qualitatively similar to observed drifter trajectories though several differences were observed. One particular trend observed was shorter predicted trajectories than observed trajectories. This is consistent with the generally lower current speeds predicted at station D2CN and D2NO relative to the ADCP data (Appendix A), though the ADCP data and drifter data were collected in different

periods. It is likely that the use of hourly wind data in the model under-estimates the effect of wind and poorly represents unsteadiness. Additional errors in predicted drifter trajectories may occur from model assumptions. The leeway factor of 0.006 is one major assumption. Similarly, the use of the water velocity at a single depth of water that corresponds to the center of the drogue kite is also approximate. The approach used is the typical approach to predict drifter trajectories (Thompson et al. 2003). More complex methods of predicting drifter trajectories are possible (Furnans et al. 2008) but can only be expected to provide increased accuracy if highly resolved and accurate hydrodynamic model results are available (Furnans et al. 2008). The observations are also imperfect, in particular because of the effects of vegetation, including several instances of immobilization of drifters. Though both the observations and modeling approach are imperfect, the model skills reported in Table 4 provide some confidence in the Lagrangian predictions.

The comparison of circulation patterns in CCF during periods of high and low winds provides a conceptual model for two distinctly different circulation regimes. During periods of high winds, a strong counterclockwise circulation gyre in CCF results in significant mixing and increases the range of estimated transit times from the radial gates to the Banks Pumping Plant. The vertical variability of wind-driven velocities also results in mixing that is manifested by a large range of estimated residence times for high wind conditions. In contrast, during higher export and low wind conditions, residence times are much shorter and increase with distance from the Banks Pumping Plant, suggesting that most particles are transported roughly in a straight-line trajectory from the radial gates to the Banks Pumping Plant. These distinctly different circulation regimes result in significantly different residence times and transit times in CCF and may account for some of the variability in the recent estimates of prescreen losses in CCF.

This hydrodynamic results presented here have several implications on management of the Delta for protection of delta smelt and other fish species. Assuming that fish residence time is related to hydrodynamics in CCF, gate operations and pumping may dramatically affect fish migration rates across CCF. Specifically, the transit time from the radial gates to the SFPF can be multiple weeks under low pumping conditions and even during moderate pumping conditions a small portion of particles entering CCF can have a large transit time, particularly during windy conditions. To the extent that fish behave as passive particles, fish that are salvaged at SFPF did not necessarily enter CCF recently and, therefore, closing the radial gates will not always immediately reduce salvage. Detailed studies of fish movement patterns and salvage are needed to determine the degree to which fish migration and loss rates are correlated to hydrodynamic conditions in CCF.

ACKNOWLEDGMENTS

This study was conducted under the auspices of the Interagency Ecological Program (IEP) for the San Francisco Estuary. The authors would like to thank Ted Sommer (CDWR) and Lenny Grimaldo (USBR) for providing project funding and management for this research through the IEP Pelagic Organism Decline (POD) program. The UnTRIM code was developed and provided by Professor Vincenzo Casulli (University of Trento, Italy). Field data used in this study were collected by Cathy Ruhl (USGS) and Jim George (USGS). Additional data and information was provided by Eli Ateljevich (CDWR), Min Yu (CDWR), Guy Masier (CDWR), Bryant Giorgi (CDWR), Tara Smith (CDWR), Shawn Mayr (CDWR), Ted Swift (CDWR), Gonzalo Castillo (USFWS), and Siqing Liu (CDWR). The RmaSim visualizer developed by RMA, Inc. was used for visualization of the particle tracking results. Rusty Holleman, Thomas Hervier, and Sandy Chang provided assistance with analysis of the particle tracking results. The authors would like to thank two anonymous reviewers for their careful review of the manuscript and suggestions for improvements.

REFERENCES

Bennett WA. 2005. Critical assessment of the delta smelt population in the San Francisco Estuary, California. San Francisco Estuary and Watershed Science [Internet]. [cited 20 October 2010]; 3(2). Available from: *http://www.escholarship.org/uc/item/0725n5vk*

CALFED, 2009. Very few marked delta smelt recovered at Skinner Fish Facility. Science News. CALFED Science Program. October 2009. Available from: *http://science.calwater.ca.gov/publications/sci_news_1009_salvage.html*

Castillo G, Morinaka J, Lindberg J, Fujimara R, Baskerville-Bridges B, Hobbs J, Tigan G, Ellison L. 2012. Pre-screen loss and fish facility efficiency for delta smelt at the State Water Project. San Francisco Estuary and Watershed Science [Internet]. [cited 20 December 2012];10(4). Available from: *http://www.escholarship.org/uc/item/28m595k4*

Casulli V. 1990. Semi-implicit finite difference methods for the two-dimensional shallow water equations. J Comput Phys 86:56-74.

Casulli V. 1999. A semi-implicit numerical method for non-hydrostatic free-surface flows on unstructured grid. Numerical Modelling of Hydrodynamic Systems, ESF Workshop. Zaragoza, Spain. p. 175-193.

Casulli V. 2009. A high-resolution wetting and drying algorithm for free surface hydrodynamics. Int J Num Meth Fluid 60(4):391-408.

Casulli V, Cheng RT. 1992. Semi-implicit finite difference methods for three-dimensional shallow water flow. Int J Num Meth Fluid 15:629-648.

Casulli V, Walters RA. 2000. An unstructured, three-dimensional model based on the shallow water equations. Int J Num Meth Fluid 32:331-348.

Casulli V, Zanolli P. 2002. Semi-implicit numerical modelling of non-hydrostatic free-surface flows for environmental problems. Math Comput Model 36:1131-1149.

Casulli V, Zanolli P. 2005. High Resolution Methods for Multidimensional Advection-Diffusion Problems in Free-Surface Hydro Ocean Model 10(1-2):137-151.

[CDWR] California Department of Water Resources, 1986. DAYFLOW program documentation and data summary user's guide. Sacramento (CA): California Department of Water Resources. 69 p. Available from: *http://www.water.ca.gov/dayflow/docs/DAYFLOW_1986.pdf*

[CDWR] California Department of Water Resources. 2005. DSM2 Delta tidal hydraulic and water quality modeling methods and results. Appendix D. South Delta Improvements Program EIS/EIR. 99 p. Available from: *http://baydeltaoffice.water.ca.gov/sdb/sdip/documents/draft_eis_eir/vol-2/doc/app_d/app_d.pdf*

Cheng RT, Casulli V, Gartner JW. 1993. Tidal residual intertidal mudflat (TRIM) model and its applications to San Francisco Bay, California. Est Coast Shelf Sci 369:235-280.

Clark KW, Bowen MD, Mayfield RB, Zehfuss KP, Taplin JD, Hanson CH. 2009. Quantification of pre-screen loss of juvenile steelhead in Clifton Court Forebay. Sacramento (CA): California Department of Water Resources. 139 p. Available from: *http://baydeltaoffice.water.ca.gov/ndelta/fishery/documents/2009_clark_et_al_quantification_of_steelhead_pre-screen_loss.pdf*

Clemmens AJ, Strelkoff TS, Replogle JA. 2003. Calibration of submerged radial gates. J Hydraul Eng 129(9):680-687.

Deleersnijder E, Beckers JM, Campin JM, El Mohajir M, Fichefet T, Luyten P. 1997. Some mathematical problems associated with the development and use of marine models. In: Diaz JI, editor. The mathematics of models for climatology and environment. Volume I 48. Berlin, Heidelberg: Springer Verlag. p. 39-86.

Dunsbergen DW. 1994. Particle models for transport in three-dimensional flow [Ph.D. dissertation]. Available from: Delft University of Technology.

Flow Science, Inc. 2005. Fischer Delta model study: fate of a conservative tracer during water years 2000-2001. FSI Report 048007. Prepared for the San Joaquin River Group Authority. 39 p. Available from: *http://www.waterrights.ca.gov/baydelta/docs/exhibits/SJRG-EXH-24.pdf*

Furnans J, Imberger J, Hodges BR. 2008. Including drag and inertia in drifter modeling. Environ Model Soft 23:714-728.

Geyer WR. 1989. Field calibration of mixed-layer drifters. J Atmos Ocean Tech 6:333-342.

Grimaldo LF, Sommer T, Van Ark N, Jones G, Holland E, Moyle PB, Herbold B, Smith P. 2009. Factors affecting fish entrainment into massive water diversions in a tidal freshwater estuary: can fish losses be managed? N Am J Fish Manage 29:1253-1270.

Gross ES, MacWilliams ML, Holleman CD, Hervier TA. 2010a. POD 3–D particle tracking modeling study. Particle tracking model testing and applications report. Available from: *http://www.science.calwater.ca.gov/pdf/workshops/POD/GrossEtAl_POD3D_Particle_tracking_2010.pdf*

Gross ES, MacWilliams ML, Kimmerer WJ. 2010b. Three-dimensional modeling of tidal hydrodynamics in the San Francisco Estuary. San Francisco Estuary and Watershed Science [Internet]. [cited 18 February 2010]; 7(2). Available from: *http://www.escholarship.org/uc/item/9rv243mg*

Hills E. 1988. New flow equations for Clifton Court gates. Technical memorandum. Sacramento (CA): California Department of Water Resources, State Water Project Division of Operations and Maintenance. May 9, 1988. 19 p.

Jones NL, Monismith SG. 2008. Modeling the influence of wave-enhanced turbulence in a shallow tide- and wind-driven water column. J Geophys Res 113, C03009. doi:10.1029/2007JC004246

[IEP] Interagency Ecological Program. 2010. DSS database. Available from: *http://www.water.ca.gov/iep/products/data.cfm*

Kano RM. 1990. Occurrence and abundance of predator fish in Clifton Court Forebay, California. Technical Report 24. Interagency Ecological Study Program for the Sacramento-San Joaquin Estuary. May 1990. 16 p.

Kantha LH, Clayson CA. 1994. An improved mixed layer model for geophysical applications. J Geophys Res 99:25235–25266.

Kimmerer WJ. 2008. Losses of Sacramento River Chinook salmon and delta smelt to entrainment in water diversions in the Sacramento-San Joaquin Delta. San Francisco Estuary and Watershed Science [Internet]. [cited 20 October 2010]; 6(2). Available from: *http://www.escholarship.org/uc/item/7v92h6fs*

Large W, Pond S. 1981. Open ocean momentum flux measurements in moderate to strong winds. J Phys Oceanog 11:324-336.

Le K. 2004. Calculating Clifton Court Forebay inflow. In: Methodology for flow and salinity estimates in the Sacramento-San Joaquin Delta and Suisun Marsh. Chapter 12. 25th Annual Progress Report. October 2004. Sacramento (CA): California Dept. of Water Resources, Delta Modeling Section. p. 12-1 to 12-13. Available from: *http://modeling.water.ca.gov/delta/reports/annrpt/2004/2004.pdf*

Le K. 2008. Delta water project operations (April through September 2008). IEP Newsletter 21(4):3. Fall 2008. Available from: *http://www.water.ca.gov/iep/newsletters/2008/IEPNewsletter_2FINALFALL2008.pdf*

Le K, Chu A. 2009. Delta water project operations (January through March 2009). IEP Newsletter 22(2):3-4. Spring 2009. Available from: *http://www.water.ca.gov/iep/newsletters/2009/IEPNewsletter_FINALSpring2009.pdf*

Lippert C, Sellerhoff F. 2007. Efficient generation of unstructured orthogonal grids. The 7th Int. Conf. on Hydroscience and Engineering (ICHE-2006), Sep. 10-Sep. 13, Philadelphia, USA.

MacWilliams ML. 2004. Three-dimensional hydrodynamic simulation of river channels and floodplains [Ph.D. dissertation]. Available from: Stanford University.

MacWilliams ML, Gross ES, 2007. UnTRIM San Francisco Bay-Delta model calibration report. Delta Risk Management Study. Prepared for the California Department of Water Resources.

MacWilliams ML, Salcedo FG, Gross ES. 2008. San Francisco Bay-Delta UnTRIM model calibration report. POD 3–D particle tracking modeling study. Prepared for the California Department of Water Resources. December 19, 2008, 344 p. Available from: *http://www.water.ca.gov/iep/docs/pod/UnTRIM_Calibration_Report.pdf*

MacWilliams ML, Salcedo FG, Gross ES. 2009. San Francisco Bay-Delta UnTRIM model calibration report. Sacramento and Stockton Deep Water Ship Channel 3–D hydrodynamic and salinity modeling study. Prepared for U.S.. Army Corps of Engineers, San Francisco District. July 14, 2009. 574 p.

Monsen NE, Cloern JE, Lucas LV, Monismith SG. 2002. A comment on the use of flushing time, residence time, and age as transport time scales. Limnol Oceanog 47(5):1545-1533.

Niiler PP, Sybrandy AS, Bi K, Poulain PM, Bitterman D. 1995. Measurements of the water-following capability of holey-sock and TRISTAR drifter. Deep Sea Res I. 42(11/12):1951-1964.

Oltmann RN, Simpson MR. 1997. Measurement of tidal flows in the Sacramento-San Joaquin Delta, California: U.S. Geological Survey. Available from: *http://sfbay.wr.usgs.gov/watershed/tidal_flow/index.html*

[RMA] Resource Management Associates. 2005. Flooded islands pre-feasibility study: RMA Delta model calibration report. Prepared for the California Department of Water Resources for submittal to the California Bay-Delta Authority.

Rossiter M. 2010. Diversions from the Delta, water years 2008 and 2009. IEP Newsletter 23(1):14-15. Winter 2010. Available from: *http://www.water.ca.gov/iep/newsletters/2010/IEPNewsletter_FinalWINTER2010.pdf*

Smith PE, Donovan JM, Wong HFN. 2005. Application of 3D hydrodynamic and particle tracking models in the San Francisco Bay-Delta Estuary. Proceedings of the 2005 World Water and Environmental Resources Congress: Anchorage, Alaska, 2005 May 15-19. American Society of Civil Engineers.

Smith PE, Oltmann RN, Smith LH. 1995. Summary report on the interagency hydrodynamic study of San Francisco Bay-Delta Estuary, California. Interagency Ecological Program for the Sacramento-San Joaquin Estuary. Technical report no. HYDRO-IATR/95-45. Sacramento (CA): California Department of Water Resources. 72 p.

Stijnen JW, Heemink AW, Lin HX. 2006. An efficient 3D particle transport model for use in stratified flow. Int J Num Meth Fluids 51:331-350.

Thompson KR, Sheng J, Smith PC, Cong L. 2003. Prediction of surface currents and drifter trajectories on the inner Scotian Shelf. J Geophys Res 108(C9). doi:10.1029/2001JC001119.

Tom B, Le K, Enright C. 2004. Dayflow Program Update. IEP Newsletter 17(1):4-6. Winter 2004. Available from: *http://www.water.ca.gov/iep/newsletters/2004/IEPNewsletter_winter2004.pdf*

Umlauf L, Burchard H. 2003. A generic length-scale equation for geophysical turbulence models. J Mar Res 61:235–265.

[USBR] U.S. Bureau of Reclamation. 2008. Sacramento-San Joaquin Delta hydrodynamic and water quality model (DSM2 Model). Appendix F: OCAP biological assessment on the continued long-term operations of the Central Valley Project and the State Water Project. 76 p. Available from: *http://www.usbr.gov/mp/cvo/OCAP/sep08_docs/Appendix_F.pdf*

[USBR] U.S. Bureau of Reclamation. 2010. Central Valley operations office reports. Delta outflow computation. Available from: *http://www.usbr.gov/mp/cvo/*

Visser A. 1997. Using random walk models to simulate the vertical distribution of particles in a turbulent water column. Mar Ecol Prog Ser 158:275-281.

Warner JC, Geyer WR, Lerczak JA. 2005a. Numerical modeling of an estuary: A comprehensive skill assessment, J Geophys Res 110. C05001. doi:10.1029/2004JC002691.

Warner JC, Sherwood CS, Arango HG, Signell RP. 2005b. Performance of four turbulence closure models implemented using a generic length scale method. Ocean Model 8:81-113.

Willmott C. 1981. On the validation of models. Phys Geog 2:184-194.